NASA TECHNICAL NOTE

NASA TN D-6964

AN EVALUATION OF SOME UNBRAKED TIRE CORNERING FORCE CHARACTERISTICS

by Trafford J. W. Leland

Langley Research Center
Hampton, Va. 23365

1. Report No. NASA TN D-6964	2. Government Accession No.	3. Recipient's Catalog No.
4. Title and Subtitle AN EVALUATION OF SOME UNBRAKED TIRE CORNERING FORCE CHARACTERISTICS		5. Report Date November 1972
		6. Performing Organization Code
7. Author(s) Trafford J. W. Leland		8. Performing Organization Report No. L-8351
9. Performing Organization Name and Address NASA Langley Research Center Hampton, Va. 23365		10. Work Unit No. 501-38-12-02
		11. Contract or Grant No.
12. Sponsoring Agency Name and Address National Aeronautics and Space Administration Washington, D.C. 20546		13. Type of Report and Period Covered Technical Note
		14. Sponsoring Agency Code

15. Supplementary Notes

16. Abstract

    An investigation to determine the effects of pavement surface condition on the cornering forces developed by a group of 6.50 × 13 automobile tires of different tread design was conducted at the Langley aircraft landing loads and traction facility. The tests were made at fixed yaw angles of 3°, 4.5^O, and 6° at forward speeds up to 80 knots on two concrete surfaces of different texture under dry, damp, and flooded conditions. The results showed that the cornering forces were extremely sensitive to tread pattern and runway surface texture under all conditions and that under flooded conditions tire hydroplaning and complete loss of cornering force occurred at a forward velocity predicted from an existing formula based on tire inflation pressure. Further, tests on the damp concrete with a smooth tire and a four-groove tire showed higher cornering forces at a yaw angle of 3° than at 4.5^O; this indicated that maximum cornering forces are developed at extremely small steering angles under these conditions.

17. Key Words (Suggested by Author(s)) Automobile tires Tire cornering forces Tire hydroplaning Surface texture	18. Distribution Statement Unclassified — Unlimited		
19. Security Classif. (of this report) Unclassified	20. Security Classif. (of this page) Unclassified	21. No. of Pages 36	22. Price* $3.00

AN EVALUATION OF SOME UNBRAKED TIRE
CORNERING FORCE CHARACTERISTICS

By Trafford J. W. Leland
Langley Research Center

SUMMARY

An investigation to determine the effects of pavement surface condition on the cornering forces developed by a group of 6.50×13 automobile tires of different tread design was conducted at the Langley aircraft landing loads and traction facility. The tests were made at fixed yaw angles of 3°, 4.5^O, and 6° at forward speeds up to 80 knots on two concrete surfaces of different texture under dry, damp, and flooded conditions. The results showed that the cornering forces were extremely sensitive to tread pattern and runway surface texture under all conditions and that under flooded conditions tire hydroplaning and complete loss of cornering force occurred at a forward velocity predicted from an existing formula based on tire inflation pressure. Further, tests on the damp concrete with a smooth tire and a four-groove tire showed higher cornering forces at a yaw angle of 3° than at 4.5^O; this indicated that maximum cornering forces are developed at extremely small steering angles under these conditions.

INTRODUCTION

Under dry operating conditions, almost any tire and runway or roadway surface provides adequate traction for vehicle stopping and for directional control at reasonable yaw angles. Under damp or wet operating conditions, however, unacceptable losses in traction may occur which depend upon combinations of speed of operation, tire tread pattern and inflation pressure, and runway water depth and surface texture. A great deal of work on wet runway braking traction loss, reported in references 1 and 2 for example, has identified at least two wet-surface phenomena which could cause serious losses in cornering force as well. These phenomena are dynamic tire hydroplaning and viscous tire hydroplaning. Dynamic tire hydroplaning, as defined in reference 3, occurs when hydrodynamic pressures built up by water trapped in the tire-ground contact area become of sufficient magnitude to lift the tire off the runway; this results in complete traction loss and wheel spin-down. Viscous tire hydroplaning generally occurs only when smooth tires are operated on smooth surfaces, and traction loss is due to the lubricating effect of a viscous film of water between tire and ground.

The purpose of this paper is to present the results of an investigation conducted at the Langley aircraft landing loads and traction facility to determine the effect of runway surface condition on the cornering forces developed by tires having different tread patterns operating unbraked at fixed yaw angles. In this investigation 6.50 × 13 automobile tires were used since the rated load was compatible with equipment limitations, and the rated tire inflation pressure resulted in an easily achievable hydroplaning speed. The tests were made at yaw angles of 3°, 4.5^O, and 6° at forward speeds up to 80 knots on two concrete surfaces of different texture under dry, damp, and flooded conditions. In addition to cornering-force-coefficient data, tire footprint photographs for nearly all test conditions were obtained through a glass plate installed in the runway surface.

SYMBOLS

Values are given in both SI and U.S. Customary Units. The measurements and calculations were made in U.S. Customary Units.

d water depth

F_C cornering force, measured normal to wheel plane

F_V vertical force

p tire inflation pressure

V forward velocity

V_H tire hydroplaning velocity

μ_C cornering force coefficient, F_C/F_V

ψ yaw angle

ω instantaneous wheel angular velocity

ω_O equivalent dry runway (synchronous) wheel angular velocity

APPARATUS AND PROCEDURE

General Description of Test Facility

The investigation was conducted at the Langley aircraft landing loads and traction facility described in reference 1. The test facility was adapted for this program as shown schematically in figure 1. The facility employs a water-jet catapult that develops up to 1800 kN (400 000 lb) thrust to accelerate the test carriage to the desired speed in a distance of about 120 m (400 ft). The carriage then coasts freely on steel rails for a distance of about 360 m (1200 ft) and is stopped at the end of the run by the arresting gear shown in figure 1. The initial carriage velocity is determined by controlling the time duration of the water jet, and during the coasting period when the tire tests are performed, the velocity decay is very small owing to the large mass, up to 289 kN (65 000 lb), of the test carriage. Paralleling the main test track is a concrete-lined channel 2.4 m (8 ft) wide and 1.5 m (5 ft) deep, which was formerly used as a water channel for high-speed hydrodynamic model testing; this channel and the small test carriage used to tow the hydrodynamic models were modified as described in the next section for use in this investigation.

Tire Test Fixture

The model towing staff of the test carriage is offset from the main carriage structure and centered over the water channel. This staff was lengthened and a fixture attached to enable the test tires to be operated on a runway surface installed in the floor of the channel. Figure 2 is an overall view of the test carriage with a fighter nose gear attached to the towing staff extension, and figure 3 is a closeup of the tire test fixture used in this investigation. This fixture employed an aircraft main landing-gear shock strut modified to hold the yoke and axle assembly depicted in figure 3 and schematically shown in figure 4(a). The shock strut was pressurized hydraulically through an accumulator whose internal volume was much larger than that of the shock strut; thus, an essentially constant down force was supplied to the yoke. The upper support structure could be rotated with respect to the test carriage and fixed at yaw angles from 0° up to about 10°.

Instrumentation

In this report, cornering force is defined as the ground force developed normal to the plane of the tire and was measured by means of the instrumentation shown in figure 4. The shock-strut assembly was attached to the staff extension at a pivot (fig. 4(a)) which allowed motion in the lateral direction only. This motion was resisted by a load cell at the top of the shock strut, located a distance A from the pivot. This load cell was oriented normal to the tire plane (fig. 4(b)) to measure cornering force directly. Since the pivot was located a distance B from the runway surface, cornering forces developed by the

tire at the runway were mechanically multiplied by the value of B/A at the load cell; this provided very sensitive and accurate load measurements.

Wheel angular velocity was measured by an axle-driven dc voltage generator. Axle vertical position was measured by a slide wire located between the upper part of the shock strut and the yoke, and vertical loads were monitored by a pressure transducer located in the hydraulic accumulator. Position of the test carriage along the track was indicated by a photocell interrupter system, with triggering provided by narrow white stripes painted at 3.05-m (10 ft) intervals on the blackened track rail support wall. All measurements were recorded as time histories on an oscillograph recorder carried on board the test carriage.

Test Runway Installation

The bottom of the water channel shown in figure 2 was judged unsuitable for tire testing because of its relatively light construction and surface unevenness. A raised, reinforced concrete test surface was therefore installed and was carefully leveled with respect to the track rail to provide minimum vertical motion of the test tire. The test strip was about 61 m (200 ft) long by 0.46 m (1.5 ft) wide and was raised off the channel floor a distance of about 10 cm (4 in.) in order to fair the concrete surface into the existing glass plate (fig. 3). The test strip consisted of five different surfaces arranged as shown schematically in figure 5. The first 15-m (50 ft) section of testing surface was covered by a steel plate 6.3 mm (0.25 in.) thick, which was coated with an antiskid compound to provide positive wheel spin-up under all wetness conditions used during the test program. The second 15-m (50 ft) section of testing surface was the original test surface and had an extremely smooth, steel-troweled finish with a surface character not unlike that commonly found on hangar or shop floors. The third 15-m (50 ft) section of test surface was provided with a fine-grained textured finish created by sand-blasting the original smooth surface. This surface, although significantly rougher than the preceding section, was still much smoother than would be acceptable for new runway or roadway construction. The fourth 15-m (50 ft) section was again the original smooth concrete surface which was faired into the glass plate that formed the fifth testing surface. This glass plate, which was approximately 1.2 m (4 ft) long, 0.9 m (3 ft) wide, and 5 cm (2 in.) thick, formed the top of a camera pit which was used in this investigation to obtain still photographs of water action in the tire footprint.

Test Tires

The tires used in this investigation were all 6.50 × 13, 4-ply-rating automobile tires having different tread patterns as shown in figure 6. The smooth tire of figure 6(a) was specially molded for this investigation and had a tread thickness equivalent to a new

tire, but had no tread pattern. The four-groove tire of figure 6(b) was also specially molded and had a tread pattern consisting of four straight, evenly spaced circumferential grooves about 4.6 mm (0.18 in.) wide and 6.3 mm (0.25 in.) deep. The tire of figure 6(c) was a standard production tire having four evenly spaced zigzag circumferential grooves also 6.3 mm (0.25 in.) deep and a regular arrangement of fine slits or sipes cut into the tread ribs. The tire of figure 6(d) was an early experimental tire of radial-ply construction, as opposed to the conventional bias-ply construction of the other test tires. The tread pattern was similar to the production tire of figure 6(c), with the addition of large zigzag grooves cut transversely into the shoulder ribs. The tires shown in figures 6(e) and (f) were similar in all respects to the four-groove tire of figure 6(b) but with the modifications shown. The four-groove dimpled tire of figure 6(e) had a series of regularly spaced 3.2-mm-diameter (0.125 in.) holes approximately 6.3 mm (0.25 in.) deep drilled in the shoulder rib, whereas the four-groove slotted tire of figure 6(f) had a series of straight slots cut into the shoulder rib at 2.5-cm (1 in.) intervals, each slot being approximately 3.2 mm (0.125 in.) wide and 6.3 mm (0.25 in.) deep.

Testing Procedures

For all phases of the test program, the tire inflation pressure was set at 18.6 N/cm^2 (27 lb/in^2) and maintained at this level through periodic checks. The vertical load was also held constant, through the hydraulic loading system described previously, at 3.71 kN (835 lb). The variable parameters for most test tires included forward velocity, yaw angle, and test surface condition, although not all tires were tested at all conditions. A set of five or six discrete, preselected forward velocities constituted one test series, with all other parameters held constant, and these velocities were in the range from 15 to 80 knots. Three yaw angles, 3°, 4.5^o, and 6°, were investigated and these angles were carefully set and fixed for a given series by using the track rail and the flat side of the support yoke as references. Three surface conditions were used in this investigation: namely, dry, damp, and flooded with water. In each case the entire 62-m (203 ft) length of the test strip was maintained at the same condition. Thus, for each surface condition and forward velocity, cornering data were obtained on both smooth and rough concrete and a tire footprint photograph was obtained. For the damp runway tests, water was applied to the surface and allowed to run off. It was found that surface tension of the water remaining created a water depth of about 1 mm (0.04 in.). This condition closely approximated a heavy morning dew, which was observed to exist on this surface during several early morning tests. For the flooded runway tests, the whole channel was filled with water to a depth of 10 mm (0.4 in.) over the test surfaces and was maintained at this level. In both the damp and flooded conditions, a sea-marker dye (sodium fluorescein) was added to the water in the glass-plate area to provide better contrast in the tire footprint photographs.

5

In the normal test procedure, the tire inflation pressure, yaw angle, and all instrumentation were checked, and the shock strut was locked in the full-up position just before launching the carriage. A knife edge was placed on the track, in a location determined by the anticipated forward speed of the carriage, to release the shock-strut lock and drop the tire on the coated-steel spin-up plate. If a damp or flooded test was proposed, water depths were checked at intervals along the test strip and sea-marker dye was added to the glass-plate area just before the carriage was launched. After launch, but before the carriage reached the test strip, the lights in the camera pit were turned on and the camera shutter was tripped by a magnetic switch activated by passage of the carriage structure when the tire was centered on the glass plate.

RESULTS AND DISCUSSION

General Comments

In the presentation and discussion of the data, the cornering force as measured normal to the tire plane has been divided by the vertical load and is expressed as cornering force coefficient μ_C. Cornering force data were obtained on the roughened concrete and the smooth concrete surfaces. Where significant differences in the data were observed between the two smooth concrete surfaces on a given run, an average value was taken. No data were obtained on the coated-steel plate owing to transients induced by impact and subsequent wheel spin-up, and no cornering force data were obtained on the glass plate because of its short length. In those areas of discussion centering on wheel spin-down due to loss of traction, the angular velocity ratio ω/ω_0 is used (where ω is the instantaneous wheel angular velocity and ω_0 is the equivalent dry runway wheel angular velocity or synchronous velocity). Yaw angle ψ for this investigation is understood to be the angle between the plane of the tire and the direction of motion.

Dry Surface Cornering Force Coefficients

The cornering force coefficients developed by four of the test tires operating on dry smooth concrete are presented in figure 7 for the three yaw angles tested. A slight increase in cornering force coefficient with increasing forward velocity is noted for all the tires as is a significant increase in cornering force coefficient with increasing yaw angle. The reason for the curious "hump" in the cornering-force-coefficient curve in the vicinity of $V = 45$ knots is not known, but it seemed to be a characteristic of all the data obtained on a dry surface. The smooth tire (fig. 7(a)) recorded the highest cornering force coefficients of this group of tires, and this is thought to be due to ground bearing pressure effects. Reference 4 states that the maximum aircraft tire-ground friction coefficient available on a dry surface is in inverse proportion to the net ground bearing pressure. Although quantitative footprint measurements unfortunately were not obtained

in this test, qualitatively the smooth tire should have the lowest net ground bearing pressure because of the absence of any tread pattern. The radial-ply tire (fig. 7(d)) developed somewhat lower cornering forces in this test than did the tires of conventional bias-ply construction. The reason for this behavior is not known although, as mentioned previously, this was an early experimental radial-ply tire and, aside from basic construction difference, there may have been differences in tread compounding materials and methods.

Similar trends in cornering force coefficient were noted for these four tires operating on the dry, roughened concrete surface, as shown in figure 8. For all these tires, a significant increase in cornering force coefficient occurs due to the relatively slight change in surface texture caused by sandblasting. Thus, it appears that cornering force coefficients are quite sensitive to small changes in surface texture; this result is similar to that noted in reference 2, which reported the effects of surface texture on braking coefficients, and to that noted in reference 5 for similar cornering tests of an aircraft tire. On both test surfaces, however, the cornering forces increase with increasing yaw angle, an indication that the yaw angle which produces maximum cornering force coefficient, as discussed in reference 5, has not been exceeded for this surface condition.

Damp Surface Cornering Force Coefficients

The presence of a very small amount of water, in this case a film approximately 1 mm (0.04 in.) thick, radically changes the behavior of tire cornering force coefficient on the smooth and roughened concrete surfaces, as shown in figures 9 and 10. For the smooth tire on damp, smooth concrete (fig. 9(a)), cornering force is seen to be almost negligible at the higher test speeds. In fact, at $\psi = 4.5^O$ some degree of wheel spin-down ($\omega/\omega_O < 1$) is noted at V = 50 and 67 knots, an indication of total traction loss. At $\psi = 3^O$ the smooth tire is seen to develop significantly higher cornering force coefficients than at $\psi = 4.5^O$, a clear indication that for these test conditions the maximum cornering force coefficient may be developed at a very small steering angle. The same sort of characteristic is shown for the four-groove tire in figure 9(b) where, at the higher forward velocities, the cornering force coefficient at $\psi = 4.5^O$ falls below that at $\psi = 3^O$, and some spin-down occurred at the highest test velocity. For the production tire of figure 9(c), no spin-down was observed, and a yaw angle of 4.5^O produced consistently higher cornering force coefficients than a yaw angle of 3°. This is thought to be an effect of sipes or knife cuts in the tire tread, which produce locally high bearing pressures at the leading edge of the sipe allowing the tire to break through the water film. On the damp surface, the radial-ply tire of figure 9(d) develops slightly higher cornering forces than the conventional production tire, except at the higher forward velocities.

The same trends are observed in figure 10 for the roughened concrete covered with 1 mm (0.04 in.) water, although the cornering force coefficients are generally higher than those for smooth concrete. Comparison of figures 9 and 10 shows that, as for the

dry condition, even a small change in surface texture has a significant effect on the damp cornering performance of this group of tires. Again, for the smooth tire in figure 10(a), a yaw angle of 3° is seen to produce higher cornering forces than a yaw angle of 4.5^O, and wheel spin-down is in evidence at the highest forward velocity. For the four-groove tire of figure 10(b), the higher yaw angle ($\psi = 4.5^O$) is also seen to produce lower cornering forces at the higher forward velocities, although in this instance no spin-down occurred.

Flooded Surface Cornering Force Coefficients

When the test concrete surfaces were flooded with water to a depth of 10 mm (0.4 in.), the cornering force coefficients developed by the test tires showed a still different characteristic as illustrated in figure 11. According to reference 3, when the water depth on the runway exceeds the tread depth of the tire, as was the condition for these tests, any tire then acts as a smooth tire and the hydroplaning velocity V_H may be predicted with good accuracy by the simple equation (from ref. 3)

$$V_H = 9\sqrt{p} \tag{1}$$

where V_H is in knots and p is the tire inflation pressure in pounds per square inch. In SI units, the equation becomes

$$V_H = 10.85\sqrt{p} \tag{2}$$

where V_H is again in knots and p is expressed in newtons per centimeter^2. For the tires of these tests with an inflation pressure of 18.6 N/cm^2 (27 lb/in^2), the predicted hydroplaning velocity is 46.8 knots and is indicated in figure 11. This prediction method was based upon experiments with a variety of tire sizes and inflation pressures, but nearly all were aircraft tires operating in the free rolling (unbraked) mode at 0° yaw angle. However, the equation quite accurately predicts the hydroplaning velocity of this group of automobile tires operating in the yawed rolling condition since, for nearly every tire, wheel spin-down and almost total loss of cornering force is noted at the predicted velocity. The spin-down noted in figures 9 and 10 is thought to be more of a viscous phenomenon rather than a dynamic fluid phenomenon owing to the extremely thin film of water present for those tests. Some authors, in fact, have drawn a distinction between "viscous tire hydroplaning," which occurs in extremely shallow water, and "dynamic tire hydroplaning," which occurs in deeper water. Equation (1) from reference 3 is based on the deeper water situation.

It is interesting to note in figure 11 that, at velocities below hydroplaning velocity, surface texture and tire tread pattern have a significant effect on the magnitude of the cornering force coefficient, although such effects are negated above hydroplaning velocity. The relatively high cornering force coefficients at the lowest forward velocities, which

8

in some instances are higher than the cornering force coefficients at the same yaw angle in shallow water (fig. 10), are probably associated with fluid drag since some portion of this force would act in a lateral direction under yawed rolling conditions.

In order to see what the effect of small tread pattern changes would be on cornering force coefficient, the four-groove tread design of figure 6(b) was modified to include small holes drilled in the shoulder rib (the four-groove dimpled tire of fig. 6(e)) and slots in the shoulder rib (the four-groove slotted tire of fig. 6(f)). The effect of these tread modifications is shown in figure 12 for damp and flooded surface conditions. The dimpled tire modification is seen to offer no significant increase in cornering force on the damp surfaces and apparently is not as effective as the standard four-groove tire on the flooded surfaces. The slotted tire, however, does show improvement in cornering force over the four-groove tire on the damp surfaces, particularly at the higher velocities. In fact, comparison with figures 9 and 10 shows that the four-groove slotted design has the highest damp cornering force coefficients of the six patterns tested. The effect of the slots is probably related to siping, in that high local bearing pressures occur at the leading edge, but the slots also offer a short escape route for water trapped in the footprint area, as is shown in the next section.

Water Action in Tire Footprint

The glass plate was used to obtain tire footprint photographs under all test conditions, and these photographs are presented in figures 13 to 24 for the six test tires under damp and flooded conditions. In each figure, the photographs are arranged in order of increasing velocity, and direction of travel is from left to right. It should be borne in mind that, although no cornering-force data were obtained on the glass plate because of its limited length, wet glass is known to be extremely slippery and thus certain tire tread distortions which are undoubtedly present on high-friction surfaces do not reveal themselves in these photographs. The water action in the footprint of the smooth tire under damp conditions, $d = 1$ mm (0.04 in.), is shown in figure 13. In the original color print from which figure 13(c) was obtained, a faint light-colored area could be discerned through the center of the footprint area, with a small trail of bubbles exiting the trailing edge of the footprint at that point. This light area is evidence of partial detachment of the tire from the surface at the relatively low forward velocity of 32.5 knots. This detachment is clearly seen in figure 13(d), obtained at $V = 42.7$ knots, where the light gray area through the center of the footprint is of significant size. Since the ground contact area of the footprint is reduced when a portion is supported by the water film and since large shear forces cannot be developed in a fluid, then the normal ground force available for developing cornering or braking forces is also reduced.

9

Further footprint detachment, to the point of almost complete separation, is evident with increasing forward velocity in figures 13(e) and (f), and the wheel angular velocity ratio ω/ω_0 is less than 1 which indicates wheel spin-down. This spin-down also occurred on the smooth concrete surface as shown in figure 9(a). The manner of footprint detachment shown in figure 13, where a tunnel effect is created by the passage of water through the center of the footprint which leaves the shoulders in contact with the surface, is quite unlike that observed for an aircraft tire in reference 3, where a general shrinkage in contact area from front to rear of the footprint occurred with increasing forward velocity. The different detachment mechanism is thought to be due to differences in construction techniques of aircraft and automobile tires, with most aircraft tires being nearly circular in cross section, whereas the automobile tire has the tread as a raised cap on top of the basic tire carcass.

The four-groove tire shown in figure 14 is seen to remain in contact with the surface until a speed of 74.8 knots is reached in figure 14(f), where a light area is seen in the center of the footprint, and spin-down ($\omega/\omega_0 < 1$) has occurred. This spin-down was also indicated on the smooth concrete surface in figure 9(b). The production tire of figure 15 and the radial-ply tire of figure 16 are seen to remain in full contact with the damp surface at all test speeds. It is interesting to note in these two figures that the knife cuts, or sipes, are clearly in evidence and appear to be full of water. The water action in the footprint of the four-groove dimpled tire is shown in figure 17. A light-shaded area at the center of the footprint and wheel spin-down are seen at $V = 72.0$ knots (fig. 17(f)), although this spin-down was not noted in the data of figure 12(a) on smooth concrete. The water action in the footprint of the four-groove slotted tire is shown in figure 18. A light area at the center of the footprint is also seen at $V = 72.0$ knots (fig. 18(f)), yet no wheel spin-down occurred and the data of figure 12(a) shows a comparatively high level of cornering force being developed on the smooth concrete. In addition to providing locally high bearing pressures, it appears from the photographs of figure 18 that the transverse slots also act to rapidly drain the shoulder rib by providing short escape paths for the water trapped between the tire and the surface. The wake patterns from these slots imply a relatively high-velocity flow through these straight grooves. No such pronounced wake flow patterns can be observed through the zigzag shoulder rib grooves in the radial-ply tire shown in figure 16.

The footprints of the tires operating in a water depth of 10 mm (0.4 in.) present a somewhat different appearance, as shown by photographs of the smooth tire in figure 19. Partial detachment of the footprint is noted in figure 19(c) at $V = 34.8$ knots, and almost complete detachment is seen in figure 19(d) at $V = 45.7$ knots, which is very close to the predicted hydroplaning velocity of 46.8 knots as indicated by a velocity ratio V/V_H of 0.98. Further increases in velocity result in total footprint detachment and wheel spin-down for the smooth tire as shown in figures 19(e) and (f). The four-groove tire in

10

figure 20 maintains contact with the surface up to $V = 36.0$ knots (fig. 20(d)), but again complete footprint detachment and wheel spin-down occur above the predicted hydroplaning velocity as shown in figures 20(e) and (f). The footprints of the production tire (fig. 21), the radial-ply tire (fig. 22), the four-groove dimpled tire (fig. 23), and the four-groove slotted tire (fig. 24) all show similar characteristics. For these tires reasonably good drainage from the footprint area is in evidence until hydroplaning velocity is exceeded and the tire loses contact with the surface.

SUMMARY OF RESULTS

It has been the purpose of this paper to present the results of an investigation of the effects of pavement surface condition on the cornering force coefficients obtained with a group of 6.50×13 automobile tires having different tread patterns. The major results of this investigation are summarized as follows:

1. Under dry surface conditions, cornering force coefficients were found to increase with increasing yaw angle ψ up to 6°, the maximum test angle, and to increase slightly with increasing forward velocity. The roughened concrete surface generally produced higher cornering force coefficients than the smooth concrete surface, with the smooth tire developing higher coefficients on both surfaces than any of the tires having a tread pattern.

2. Under damp surface conditions, with a water depth of 1 mm (0.04 in.) the smooth tire and the four-groove tire developed higher cornering forces at $\psi = 3^O$ than at $\psi = 4.5^O$, an indication that maximum cornering forces are developed at extremely small steering angles under these conditions. Some wheel spin-down was also noted for these two tires at the higher test velocities, with all the test tires showing a significant decrease in cornering force with an increase in forward velocity.

3. Under flooded conditions, with a water depth of 10 mm (0.4 in.), the hydroplaning velocity equation based upon experiments with freely rolling aircraft tires at 0° yaw angle was found to predict quite accurately the hydroplaning velocity for this group of automobile tires operating unbraked at fixed yaw angles. Above the hydroplaning velocity, all test tires suffered spin-down and nearly total loss of cornering force.

4. Under all test conditions (except above the hydroplaning velocity on flooded surfaces), higher cornering forces were developed on the roughened concrete surface than on the smooth concrete. On either surface when damp, cornering forces displayed a sensitivity to tread pattern, with the four-groove slotted tire being somewhat better than the other tread patterns. On the flooded surfaces a minor effect of tread pattern was observed only below the hydroplaning velocity.

5. The tire footprint photographs showed a characteristic footprint detachment for the flooded surface conditions, with the center portion of the footprint losing contact with

the surface first. Partial footprint detachment of the smooth tire was noted at very low forward velocity, with total detachment occurring for all tires at velocities above the predicted hydroplaning velocity.

Langley Research Center,
    National Aeronautics and Space Administration,
        Hampton, Va., October 3, 1972.

REFERENCES

1. Horne, Walter B.; and Leland, Trafford J. W.: Influence of Tire Tread Pattern and Runway Surface Condition on Braking Friction and Rolling Resistance of a Modern Aircraft Tire. NASA TN D-1376, 1962.

2. Leland, Trafford J. W.; Yager, Thomas J.; and Joyner, Upshur T.: Effects of Pavement Texture on Wet-Runway Braking Performance. NASA TN D-4323, 1968.

3. Horne, Walter B.; and Dreher, Robert C.: Phenomena of Pneumatic Tire Hydroplaning. NASA TN D-2056, 1963.

4. Smiley, Robert F.; and Horne, Walter B.: Mechanical Properties of Pneumatic Tires With Special Reference to Modern Aircraft Tires. NASA TR R-64, 1960. (Supersedes NACA TN 4110.)

5. Byrdsong, Thomas A.: Experimental Investigation of the Directional Control Capability of 18 × 5.5, Type VII, Aircraft Tires on Wet Surfaces. NASA TN D-6202, 1971.

12
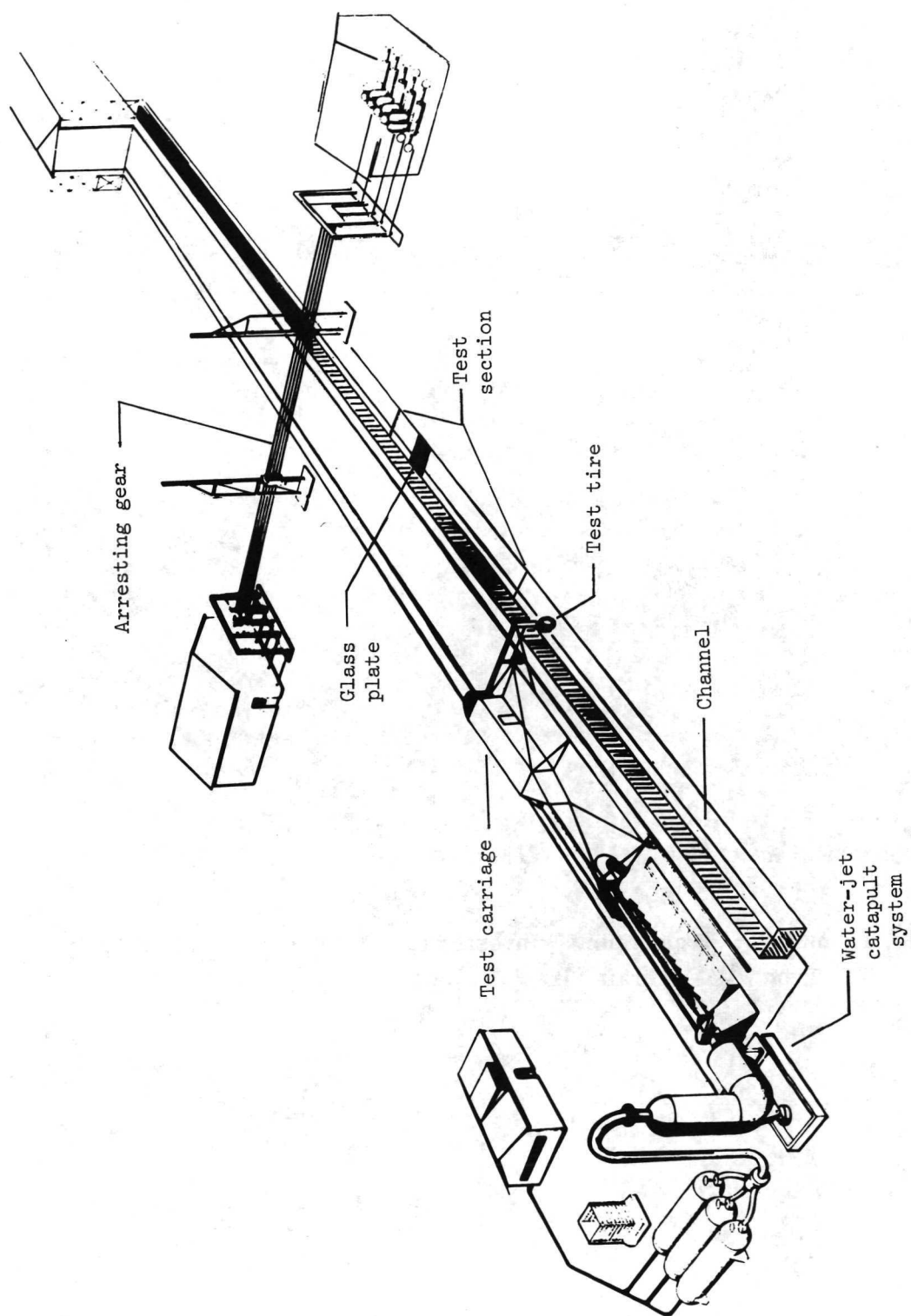
Figure 1.- Schematic of Langley aircraft landing loads and traction facility.

Arresting gear

Test section

Glass plate

Test tire

Test carriage

Channel

Water-jet catapult system

Test carriage

Water channel
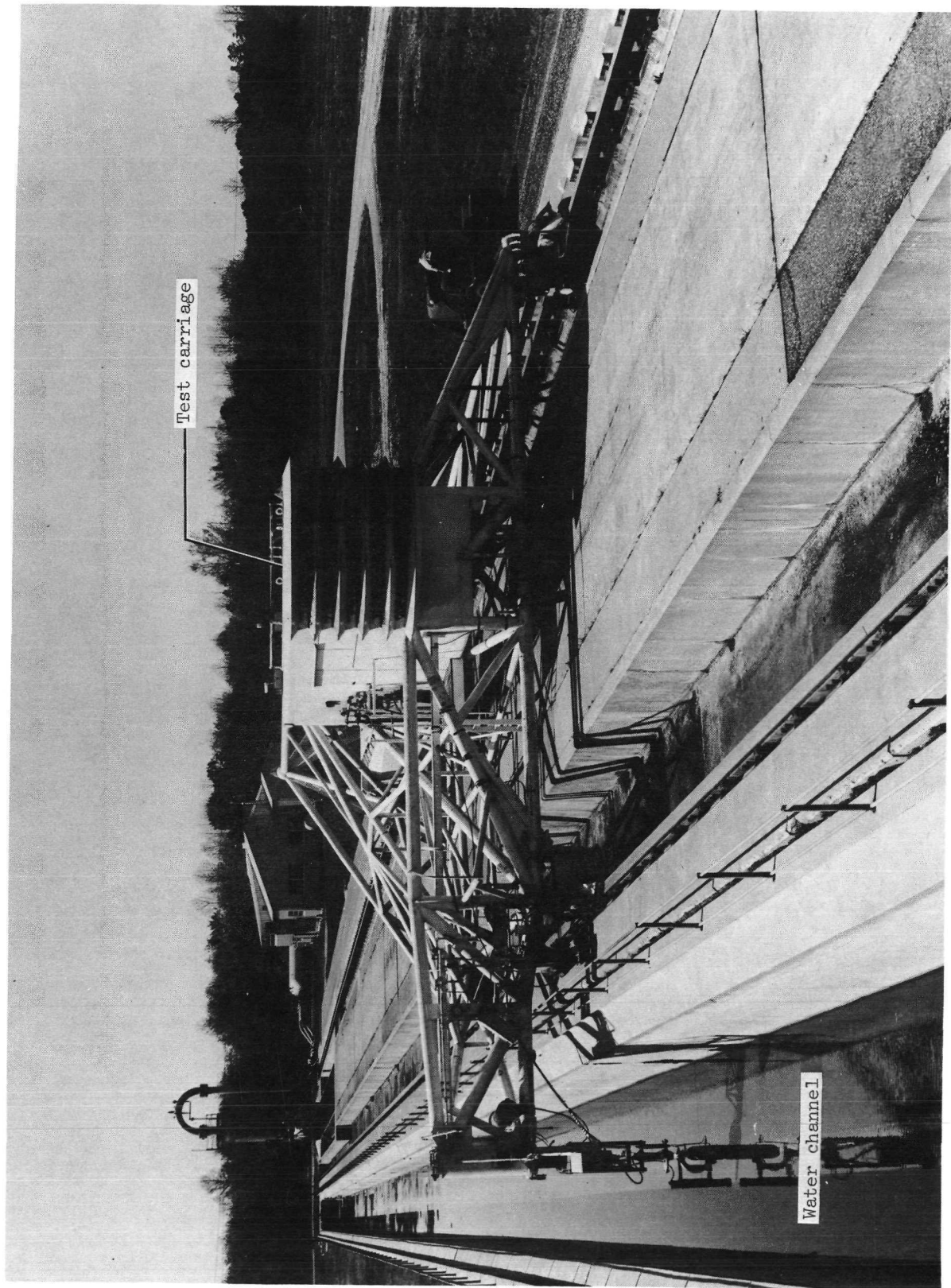
L-72-6515

Figure 2.- Overall view of test carriage and water channel.

14

Level concrete surface

Test fixture

Glass plate
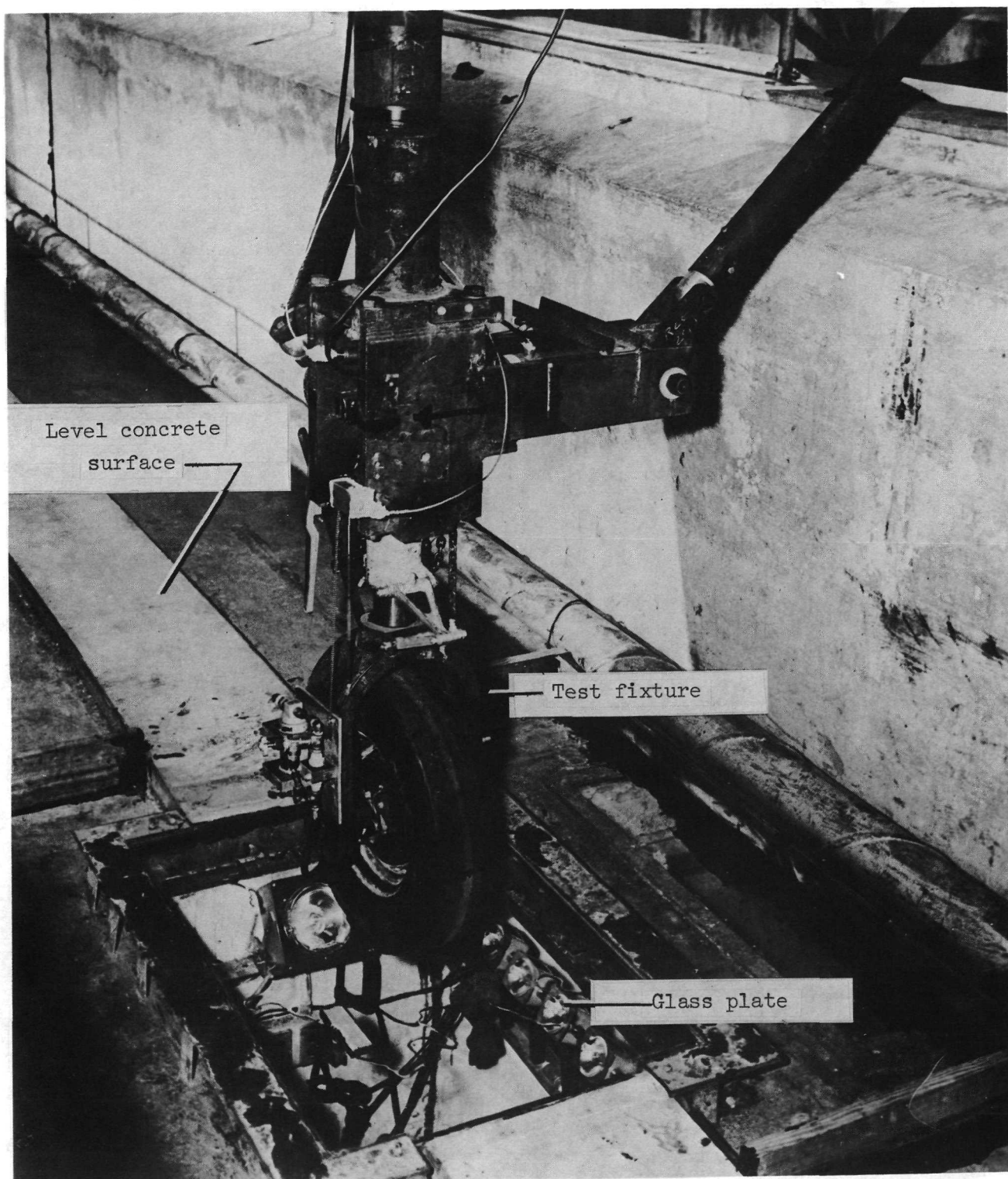
L-72-6516

Figure 3.- Closeup of test fixture with automobile tire installed.
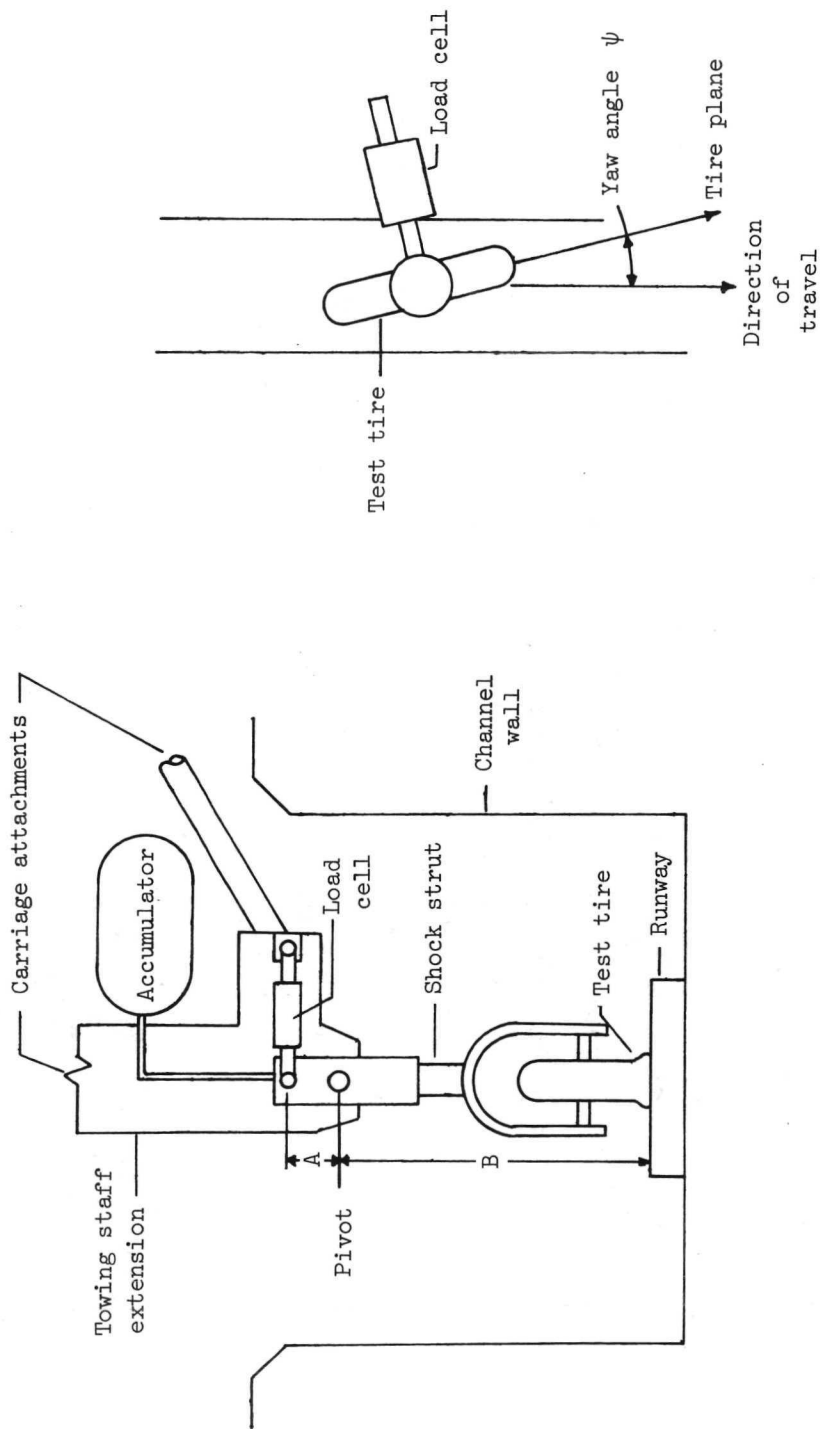
(a) Elevation view.

(b) Plan view.

Figure 4.- Schematic of tire test fixture used in this investigation.
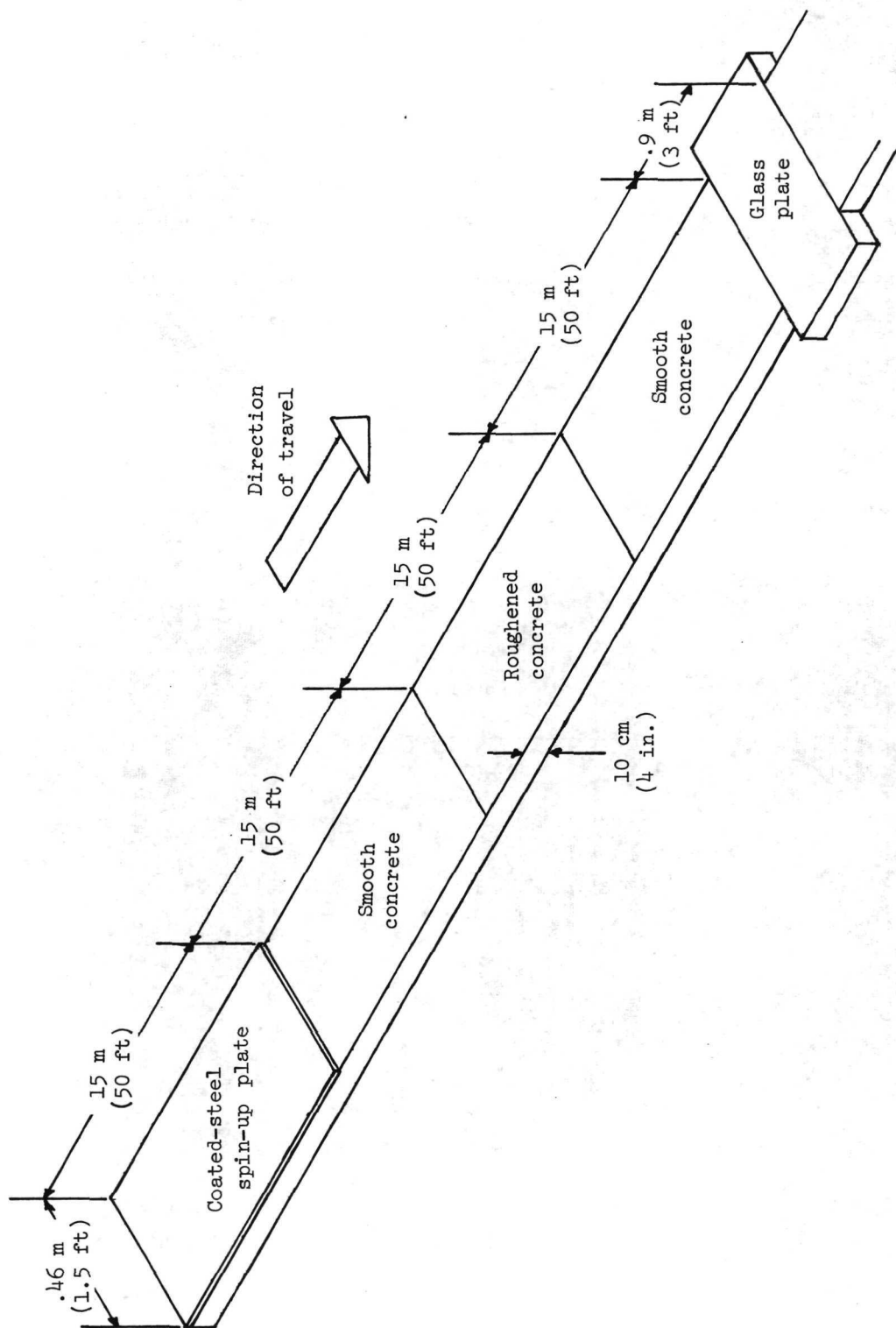
Figure 5.- Schematic of test surface arrangement.

15 m (50 ft)

.46 m (1.5 ft)

Coated-steel spin-up plate

Smooth concrete

15 m (50 ft)

Direction of travel

15 m (50 ft)

Roughened concrete

10 cm (4 in.)

15 m (50 ft)

Smooth concrete

.9 m (3 ft)

Glass plate
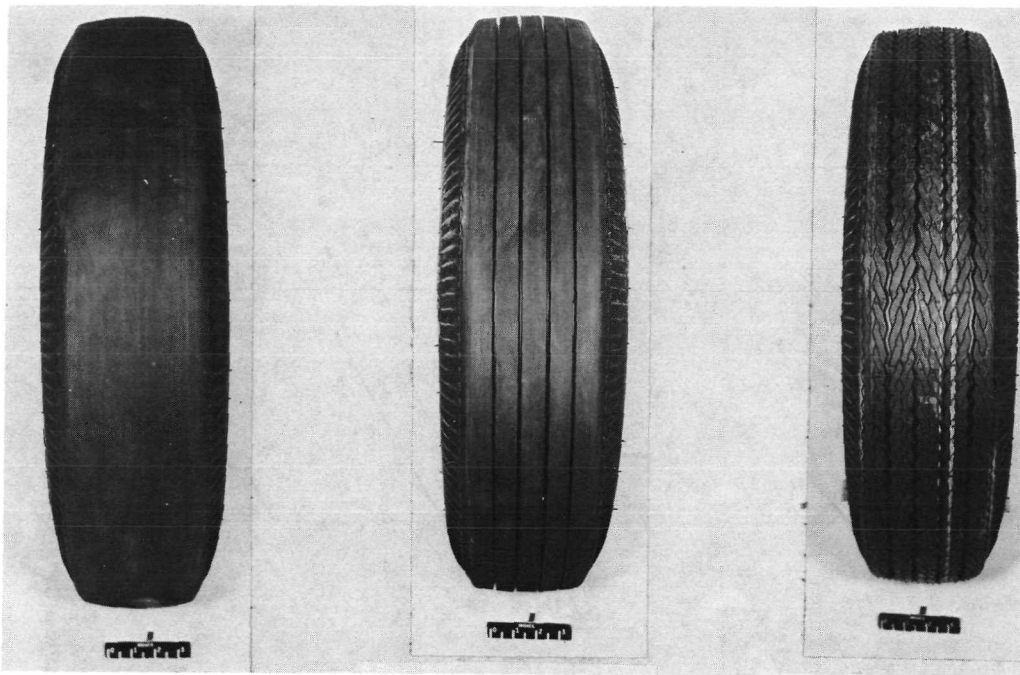
(a) Smooth tire.   (b) Four-groove tire.   (c) Production tire.
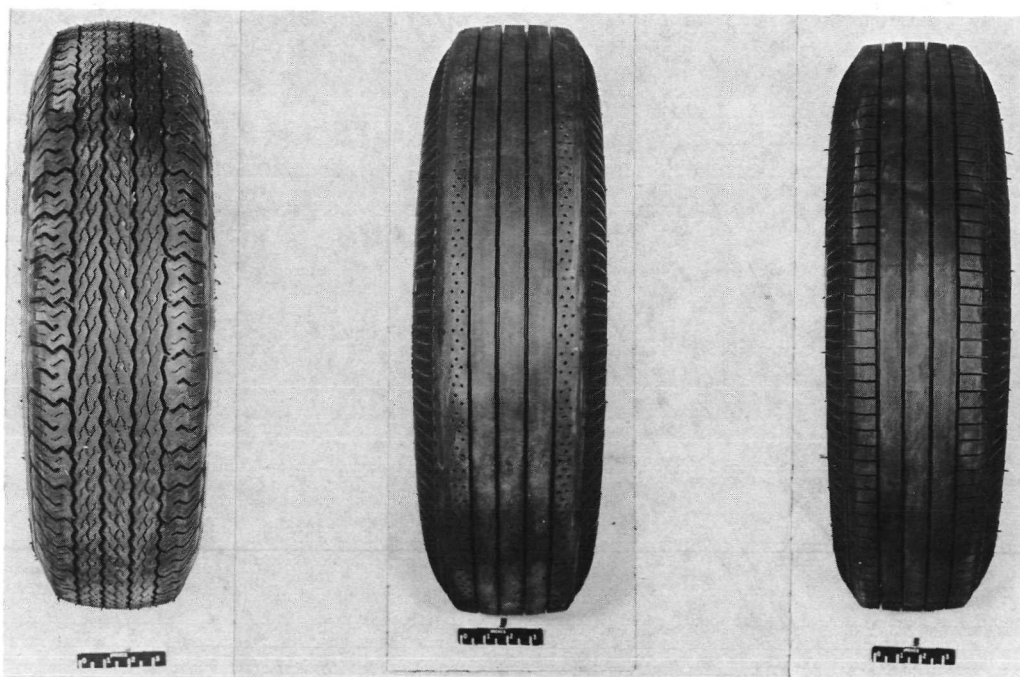
(d) Experimental   (e) Four-groove   (f) Four-groove
radial-ply tire.   dimpled tire.   slotted tire.

L-72-6517

Figure 6.- Photographs of 6.50 × 13, 4-ply-rating, automobile tires
used in this investigation.
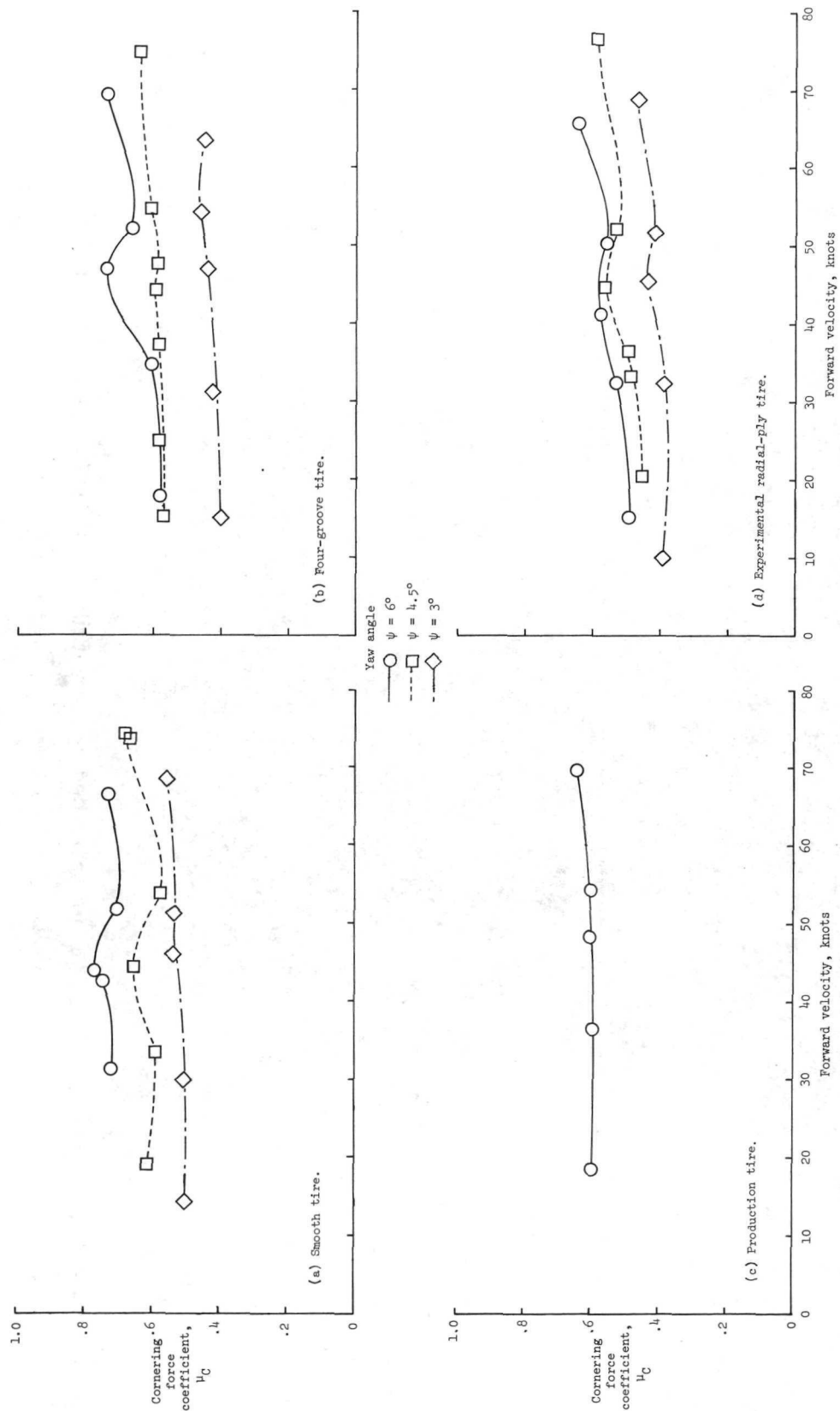
Figure 7.- Cornering force coefficients developed by four of the test tires on dry smooth concrete surface. $p = 18.6$ N/cm^2 (27 lb/in^2); $F_V = 3.71$ kN (835 lb).

19
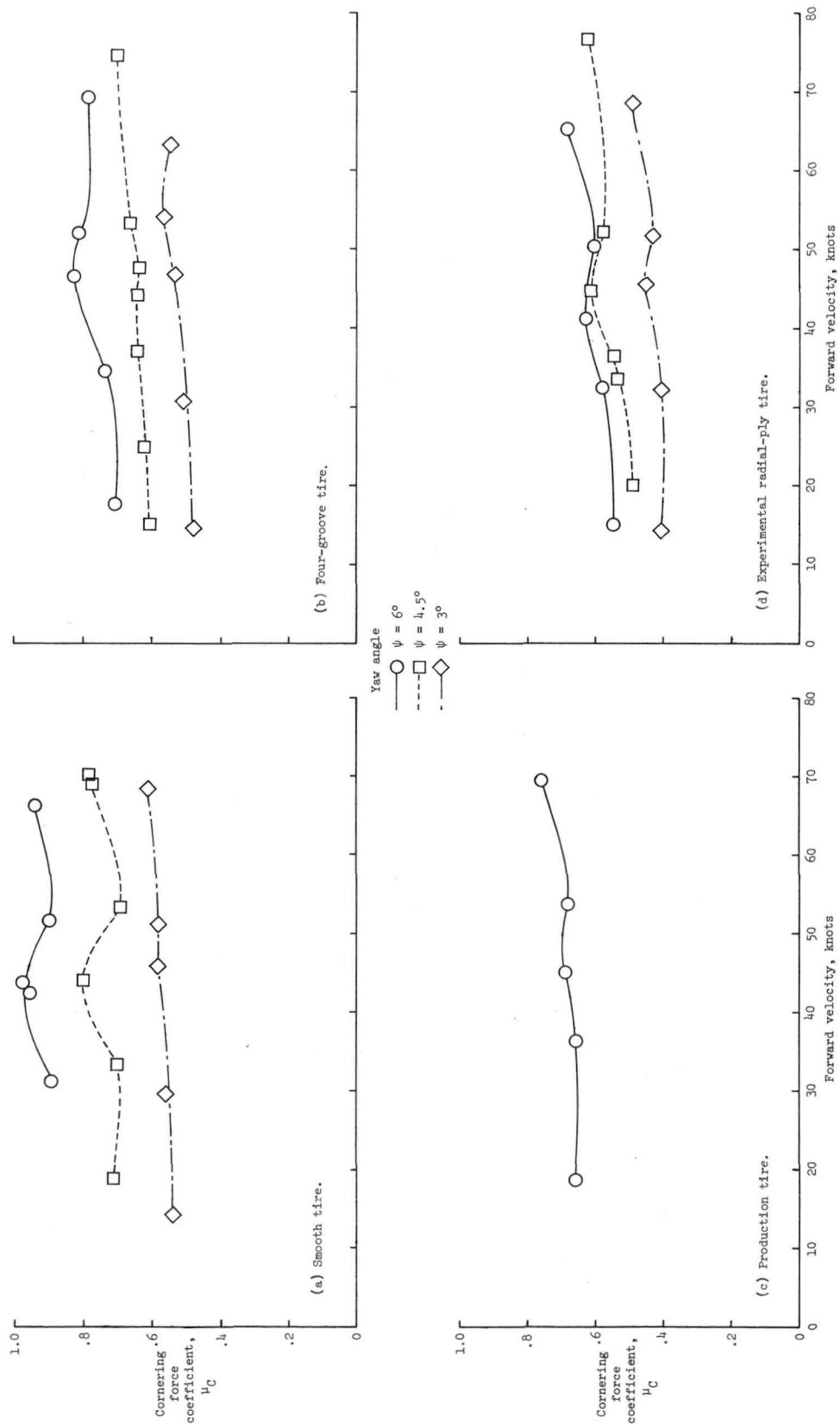
Figure 8.- Cornering force coefficients developed by four of the test tires on dry roughened concrete surface. $p = 18.6 \text{ N/cm}^2$ (27 lb/in^2); $F_V = 3.71$ kN (835 lb).
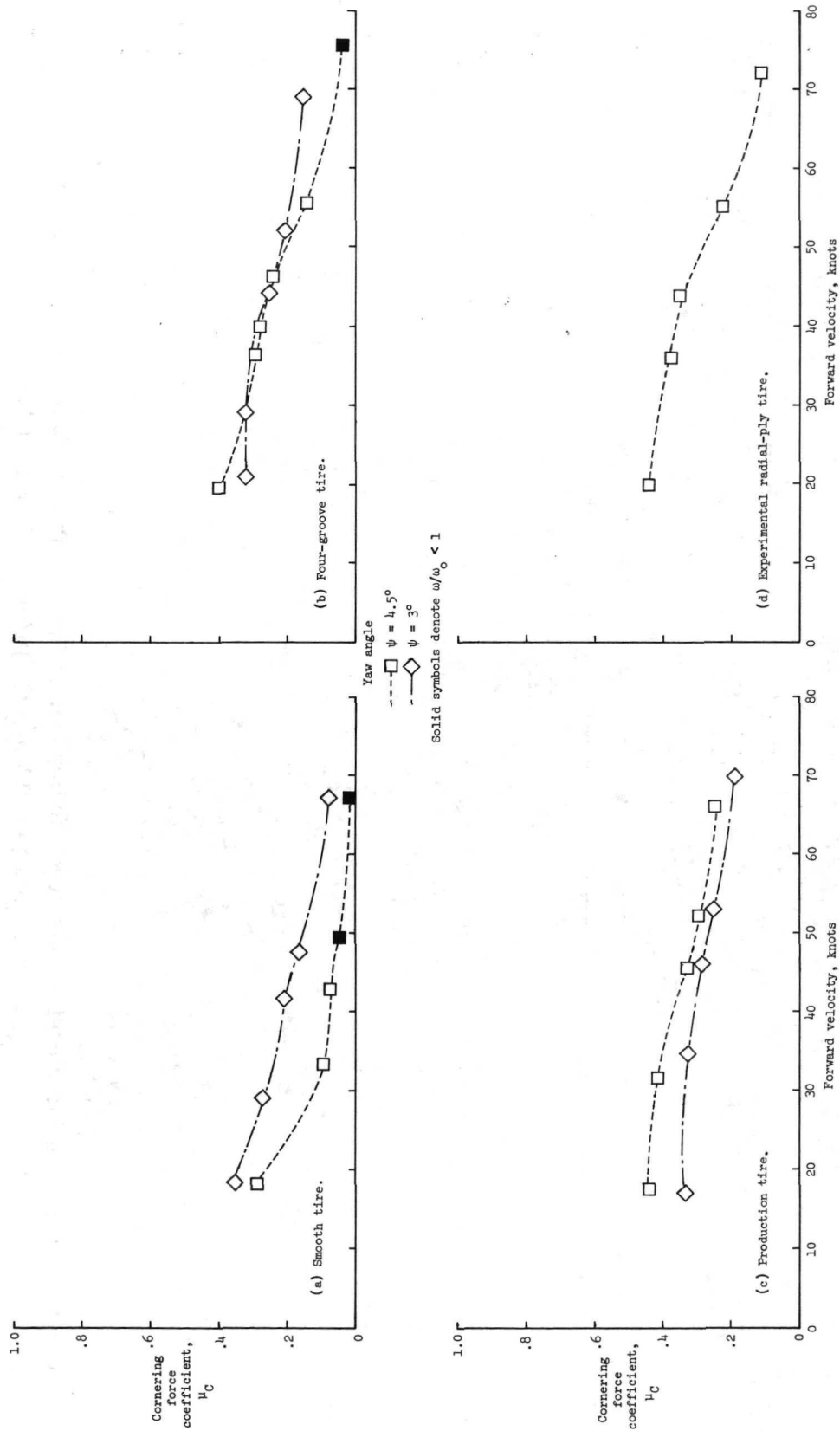
Figure 9.- Cornering force coefficients developed by four of the test tires on damp smooth concrete surface. d = 1 mm (0.04 in.); p = 18.6 N/cm² (27 lb/in²); F_V = 3.71 kN (835 lb).

21
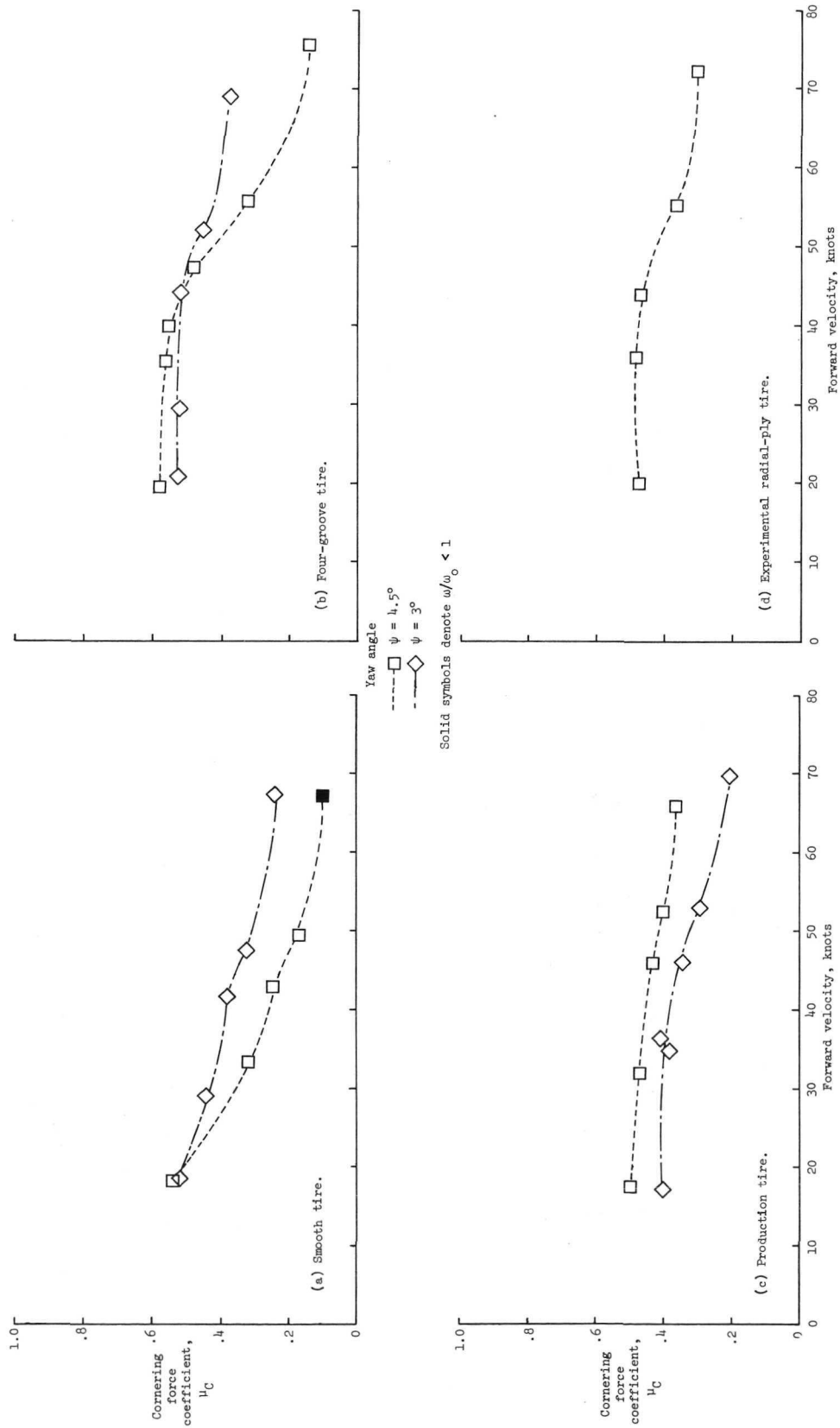
Figure 10.- Cornering force coefficients developed by four of the test tires on damp roughened concrete surface. $d = 1$ mm (0.04 in.); $p = 18.6$ N/cm^2 (27 lb/in^2); $F_V = 3.71$ kN (835 lb).

22
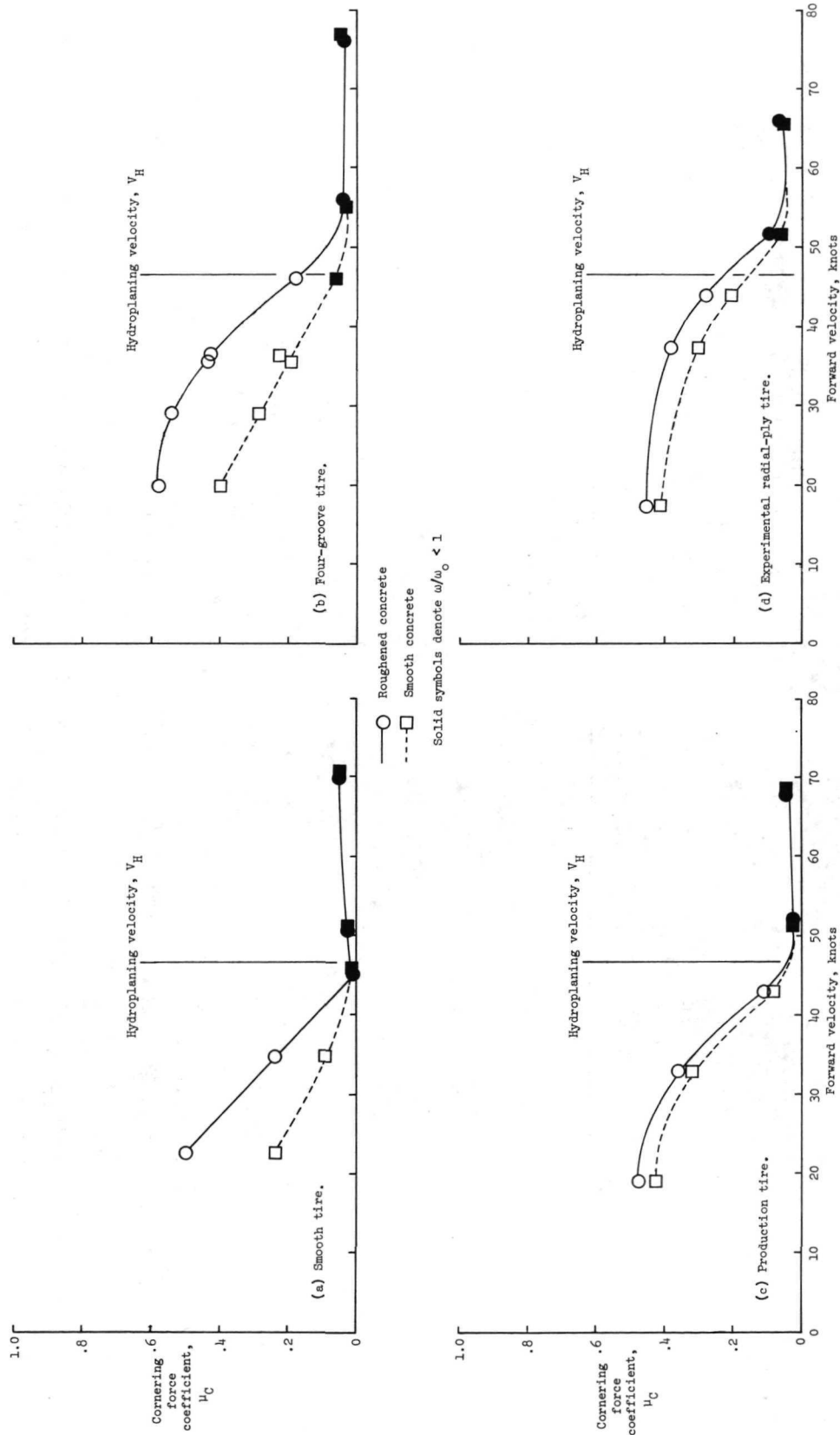
Figure 11.- Cornering force coefficients developed at $\psi = 4.5°$ by four of the test tires on flooded smooth and roughened concrete surfaces. $d = 10$ mm (0.4 in.); $p = 18.6$ N/cm^2 (27 lb/in^2); $F_V = 3.71$ kN (835 lb).
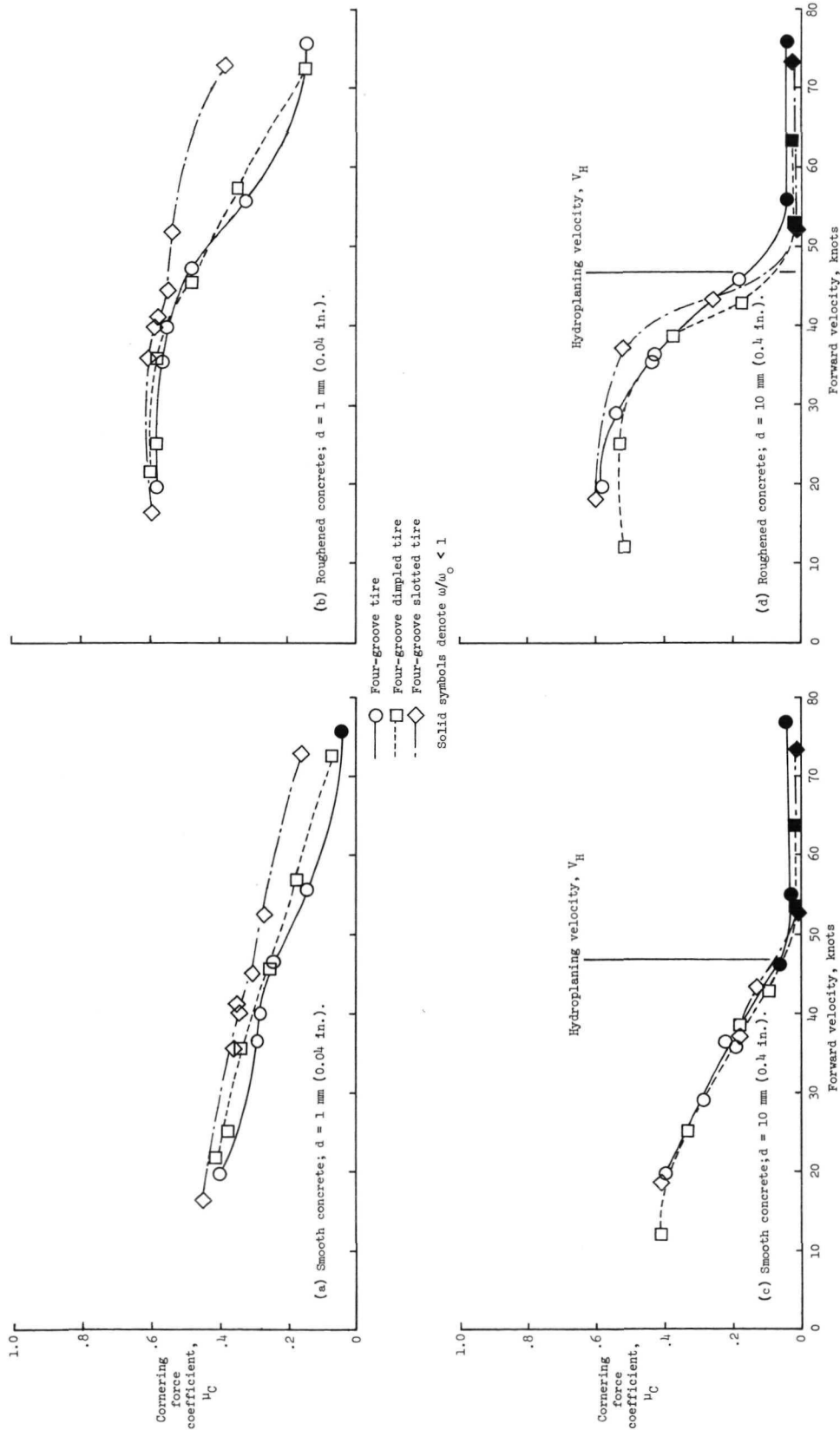
Figure 12.- Cornering force coefficients developed at $\psi = 4.5°$ by the four-groove and four-groove modified test tires on damp and flooded surfaces. $p = 18.6 \text{ N/cm}^2$ (27 lb/in²); $F_V = 3.71$ kN (835 lb).
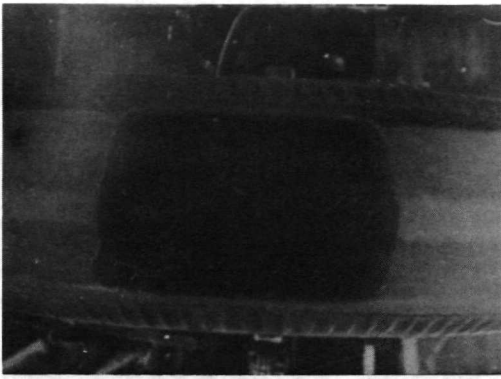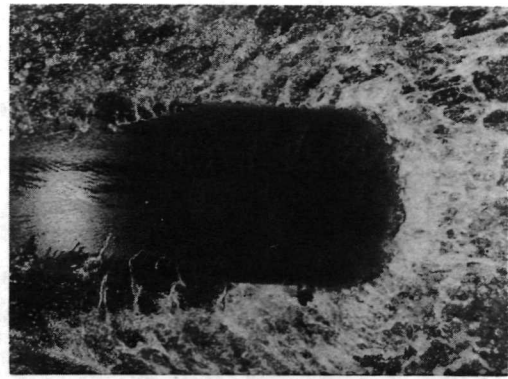
(a) Tire at rest.

(b) V = 17.6 knots; $\omega/\omega_0 = 1$.
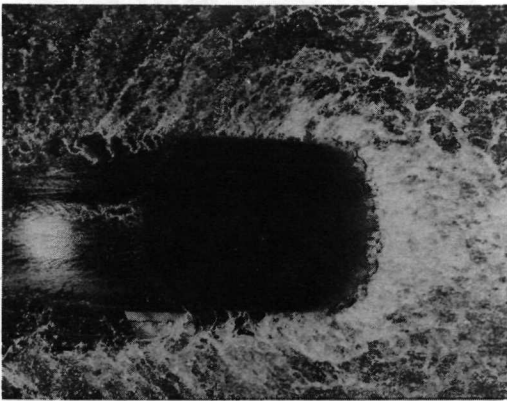
(c) V = 32.5 knots; $\omega/\omega_0 = 1$.
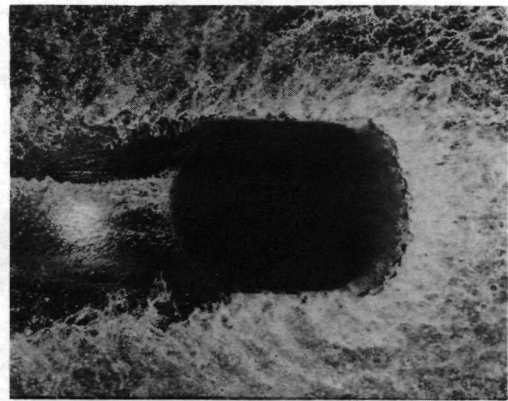
(d) V = 42.7 knots; $\omega/\omega_0 = 1$.
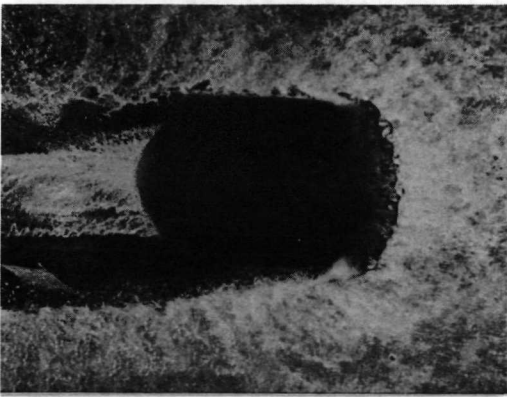
(e) V = 49.0 knots; $\omega/\omega_0 < 1$.
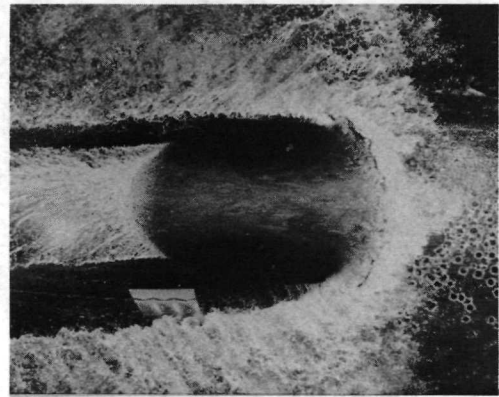
(f) V = 66.6 knots; $\omega/\omega_0 < 1$.
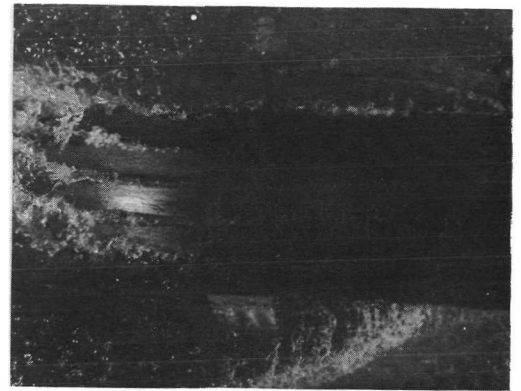
Direction of travel ⟶

L-72-6518

Figure 13.- Water action in footprint of smooth tire at   d = 1 mm (0.04 in.).
$\psi = 4.5^o$;   p = 18.6 N/cm^2 (27 lb/in^2); F_V = 3.71 kN (835 lb).
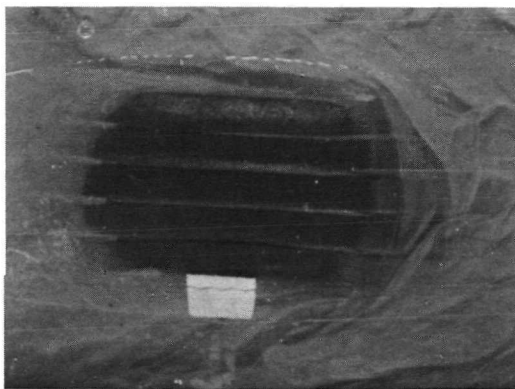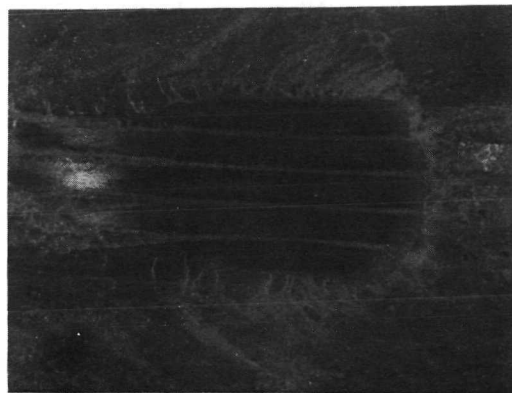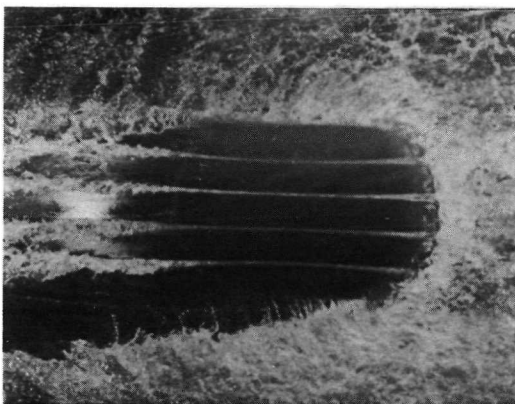
25

(a) Tire at rest.

(b) V = 19.5 knots; $\omega/\omega_O = 1.$

(c) V = 36.1 knots; $\omega/\omega_O = 1.$
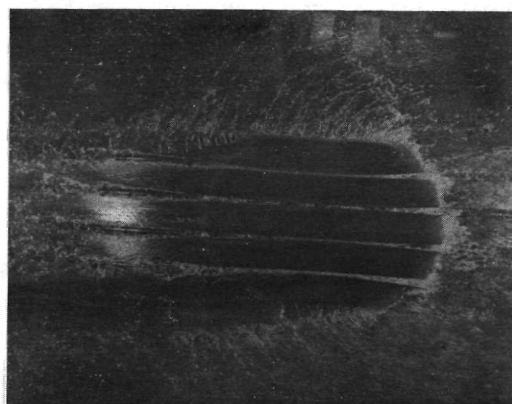
(d) V = 46.9 knots; $\omega/\omega_O = 1.$
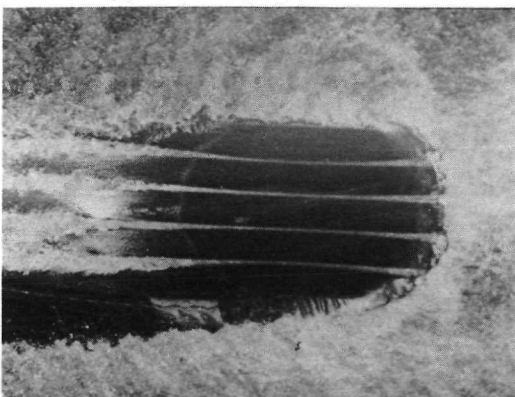
(e) V = 54.9 knots; $\omega/\omega_O = 1.$
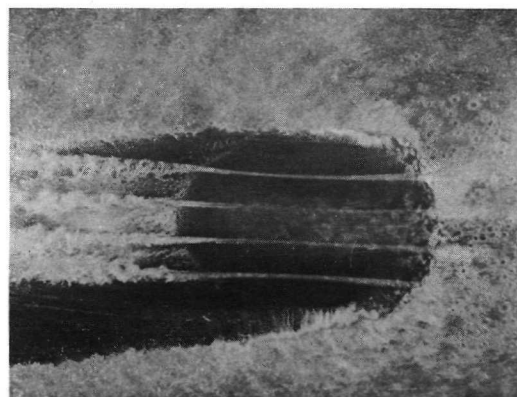
(f) V = 74.8 knots; $\omega/\omega_O < 1.$

Direction of travel ⟶

Figure 14.- Water action in footprint of four-groove tire at d = 1 mm (0.04 in.).
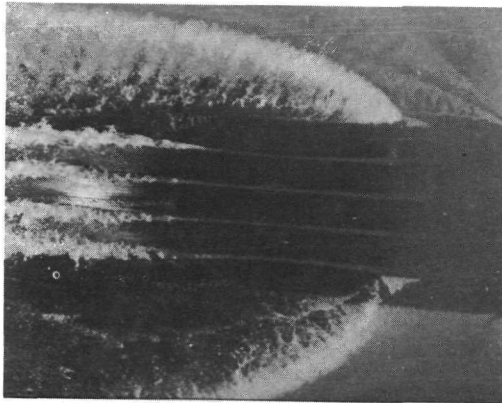$\psi = 4.5^O$; p = 18.6 N/cm^2 (27 lb/in^2); F_V = 3.71 kN (835 lb).
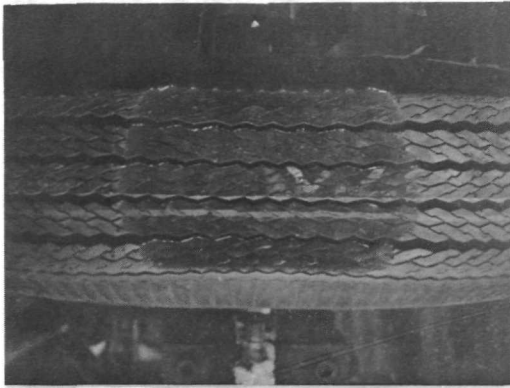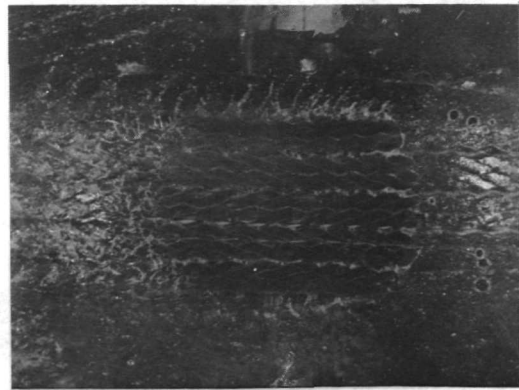
(a) Tire at rest.

(b) $V = 17.2$ knots; $\omega/\omega_0 = 1$.
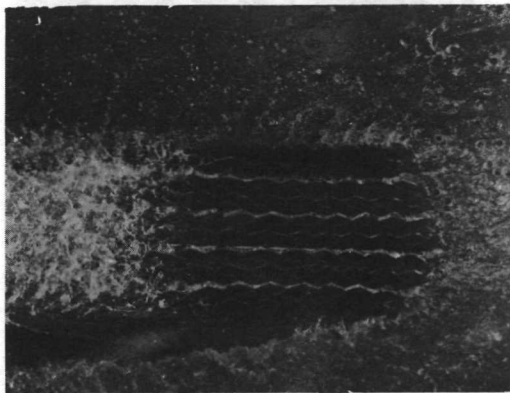
(c) $V = 31.5$ knots; $\omega/\omega_0 = 1$.
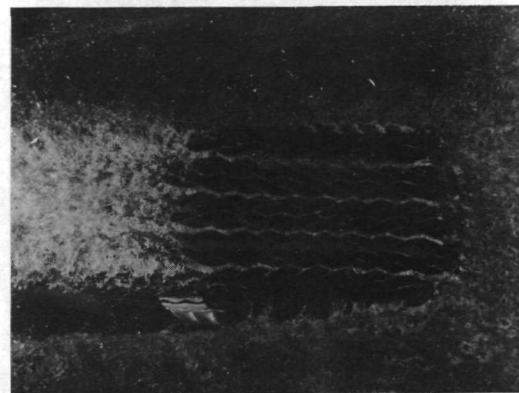
(d) $V = 45.3$ knots; $\omega/\omega_0 = 1$.
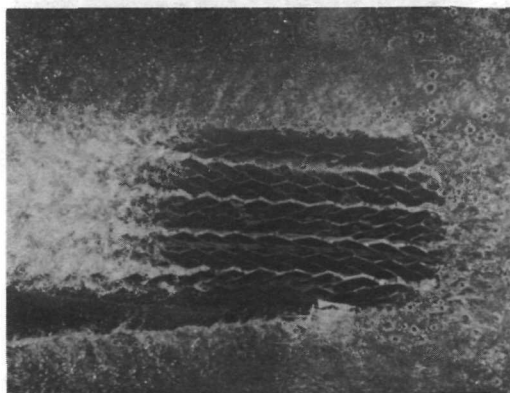
(e) $V = 52.1$ knots; $\omega/\omega_0 = 1$.
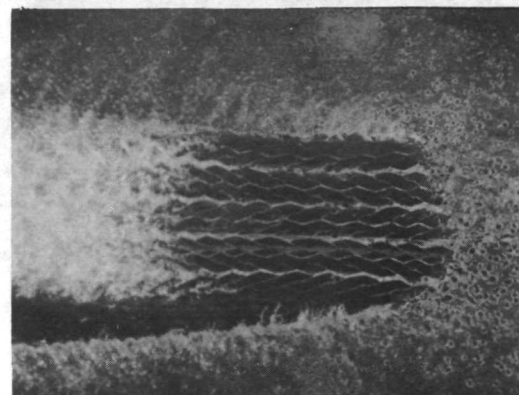
(f) $V = 65.4$ knots; $\omega/\omega_0 = 1$.

Direction of travel ⟶

L-72-6520

Figure 15.- Water action in footprint of production tire at $d = 1$ mm (0.04 in.). $\psi = 4.5^o$; $p = 18.6$ N/cm^2 (27 lb/in^2); $F_V = 3.71$ kN (835 lb).
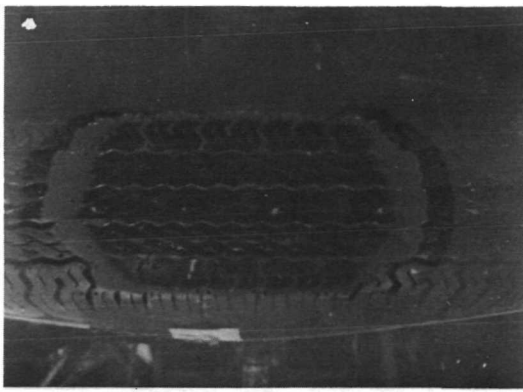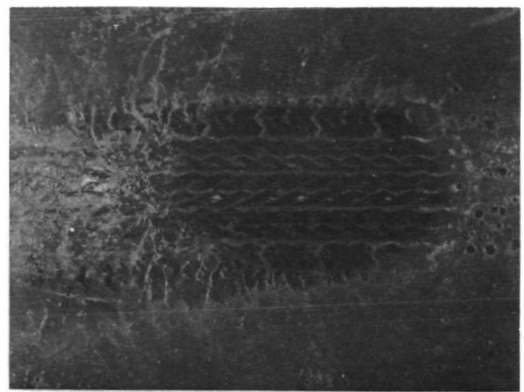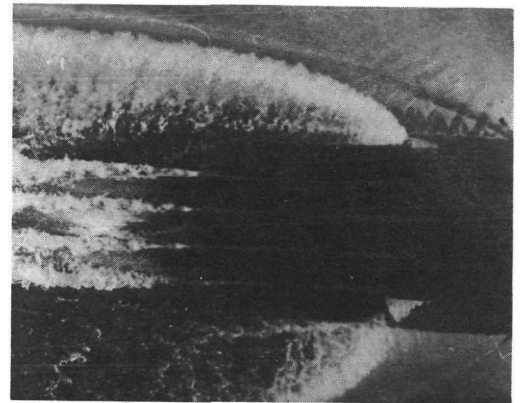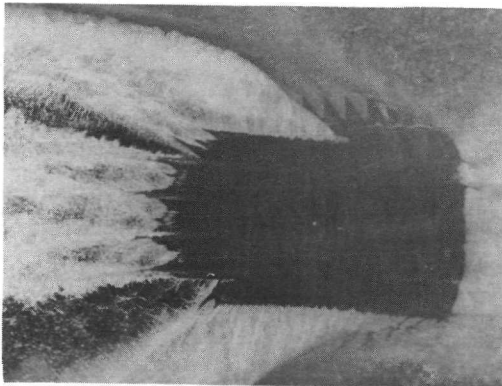
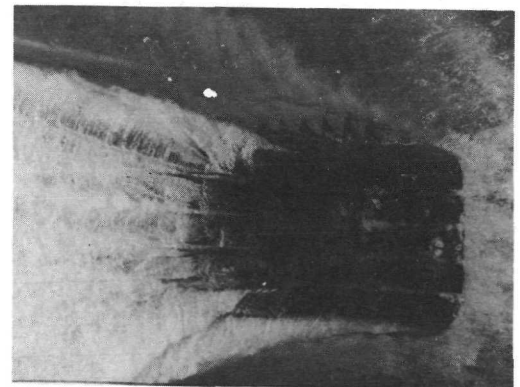(a) Tire at rest.

(b) $V = 19.5$ knots; $\omega/\omega_O = 1$.
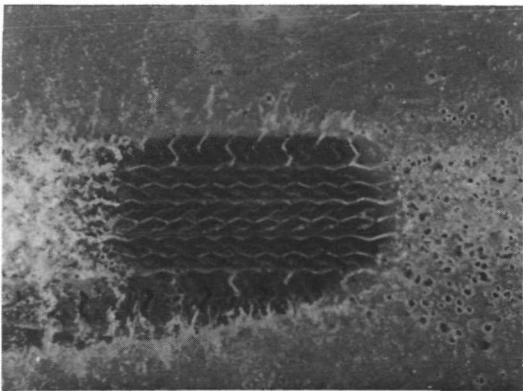
(c) $V = 36.1$ knots; $\omega/\omega_O = 1$.
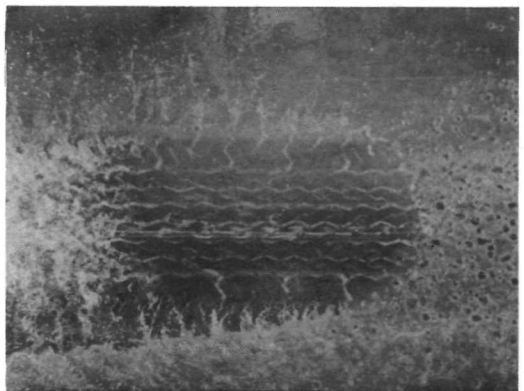
(d) $V = 43.8$ knots; $\omega/\omega_O = 1$.
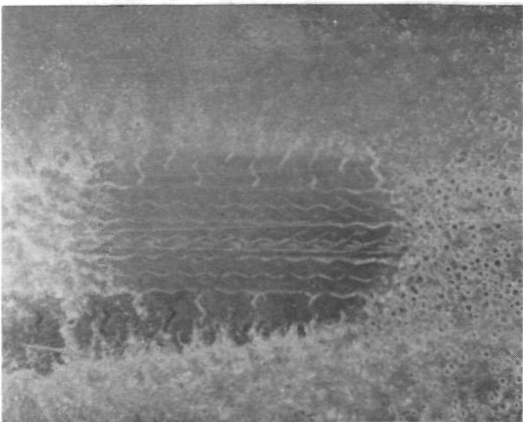
(e) $V = 54.8$ knots; $\omega/\omega_O = 1$.
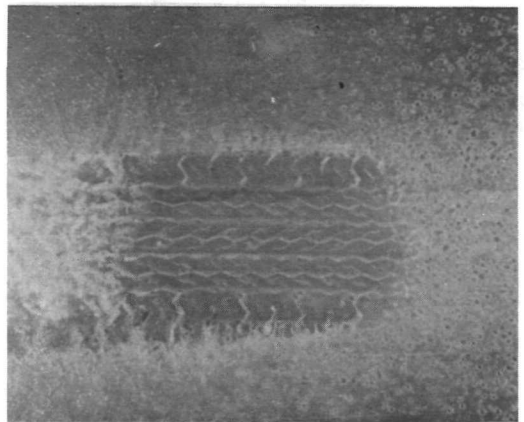
(f) $V = 71.4$ knots; $\omega/\omega_O = 1$.

Direction of travel ⟶

L-72-6521

Figure 16.- Water action in footprint of experimental radial-ply tire
at $d = 1$ mm (0.04 in.). $\psi = 4.5^O$; $p = 18.6$ N/cm^2 (27 lb/in^2);
$F_V = 3.71$ kN (835 lb).
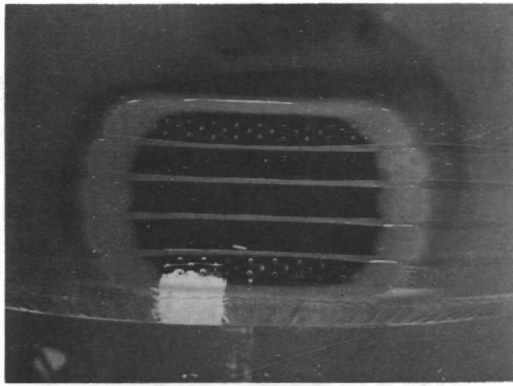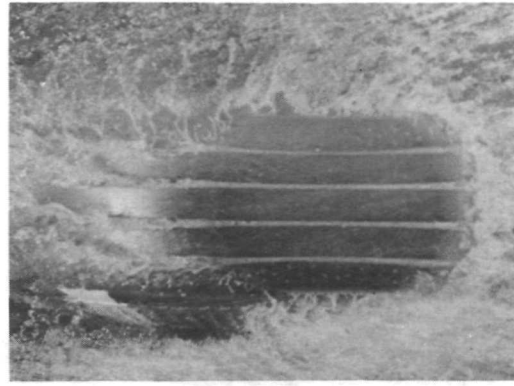
(a) Tire at rest.

(b) V = 21.5 knots; $\omega/\omega_0 = 1$.
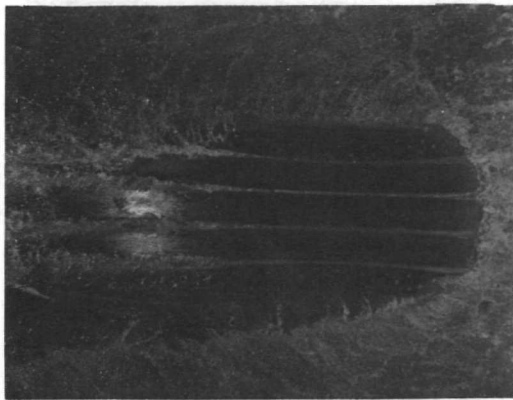
(c) V = 35.7 knots; $\omega/\omega_0 = 1$.
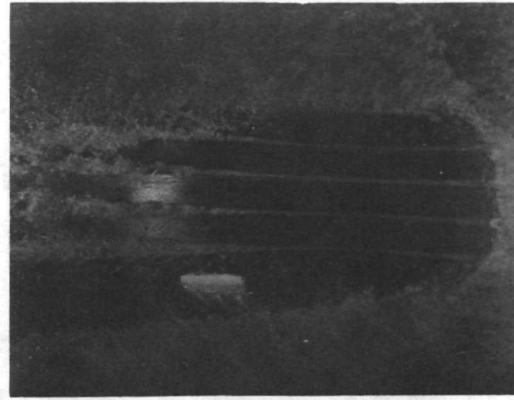
(d) V = 45.1 knots; $\omega/\omega_0 = 1$.
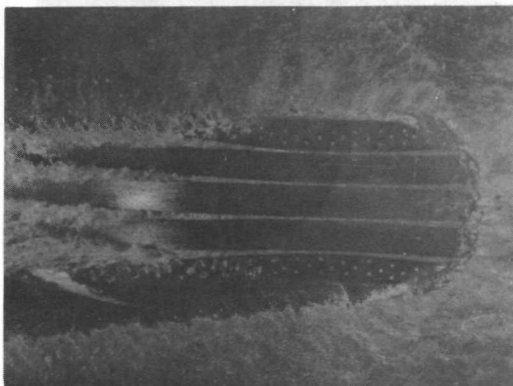
(e) V = 56.3 knots; $\omega/\omega_0 = 1$.
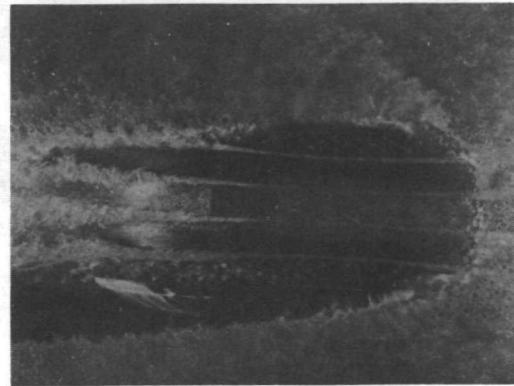

(f) V = 72.0 knots; $\omega/\omega_0 < 1$.
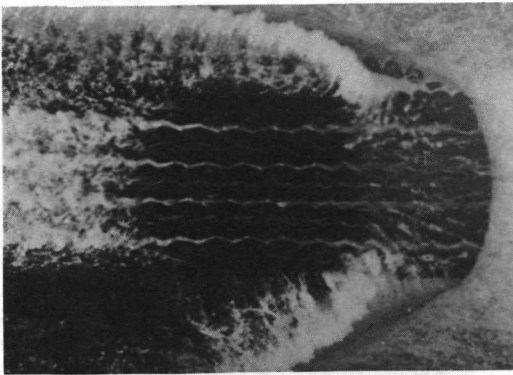
Direction of travel ⟶

L-72-6522

Figure 17.- Water action in footprint of four-groove dimpled tire at d = 1 mm (0.04 in.).
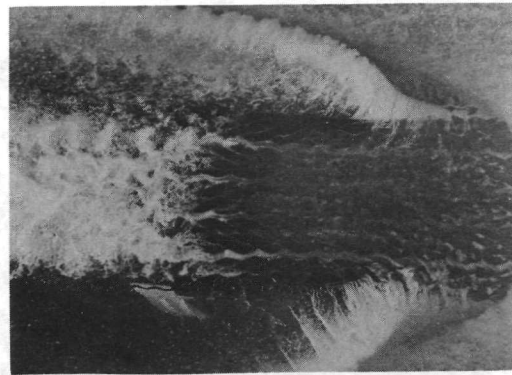$\psi = 4.5^{\circ}$; p = 18.6 N/cm^2 (27 lb/in^2); F_V = 3.71 kN (835 lb).

29
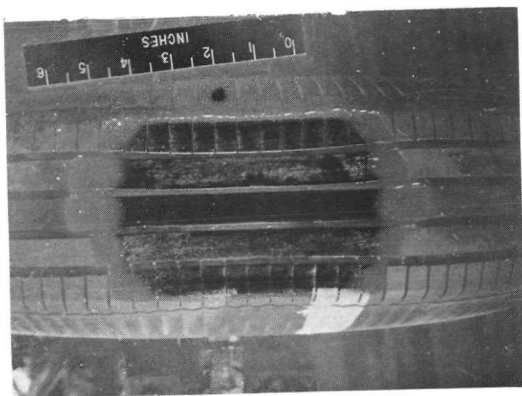
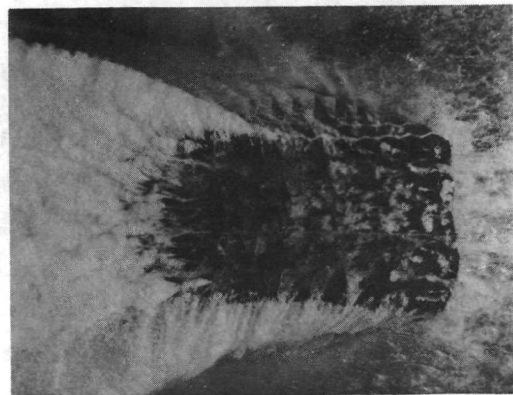(a) Tire at rest.

(b) $V = 15.6$ knots; $\omega/\omega_O = 1$.

(c) $V = 35.5$ knots; $\omega/\omega_O = 1$.

(d) $V = 44.5$ knots; $\omega/\omega_O = 1$.

(e) $V = 51.4$ knots; $\omega/\omega_O = 1$.
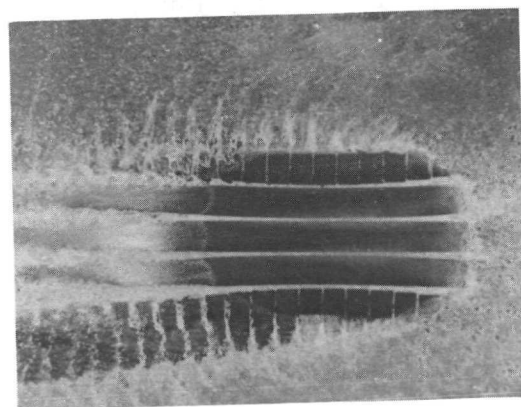
(f) $V = 72.0$ knots; $\omega/\omega_O = 1$.

Direction of travel ⟶

L-72-6523

Figure 18.- Water action in footprint of four-groove slotted tire at $d = 1$ mm (0.04 in.) $\psi = 4.5°$; $p = 18.6$ N/cm^2 (27 lb/in^2); $F_V = 3.71$ kN (835 lb).
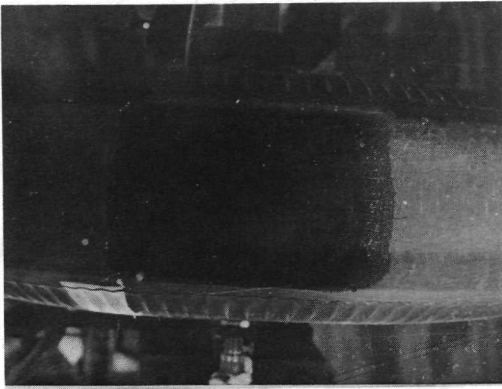
(a) Tire at rest.
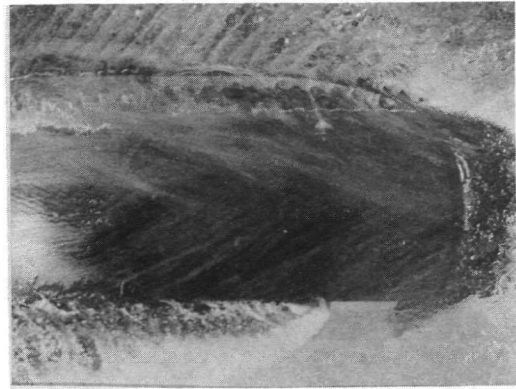
(b) $V = 22.0$ knots; $V/V_H = 0.47$; $\omega/\omega_O = 1$.
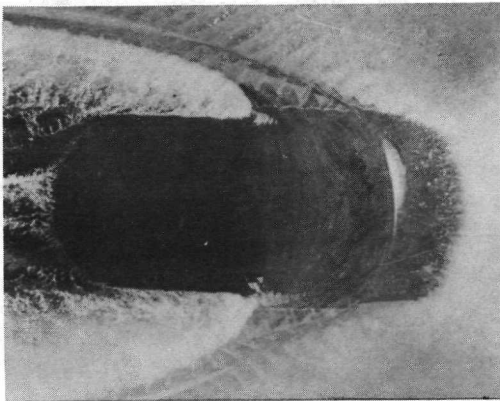
(c) $V = 34.8$ knots; $V/V_H = 0.74$; $\omega/\omega_O = 1$.
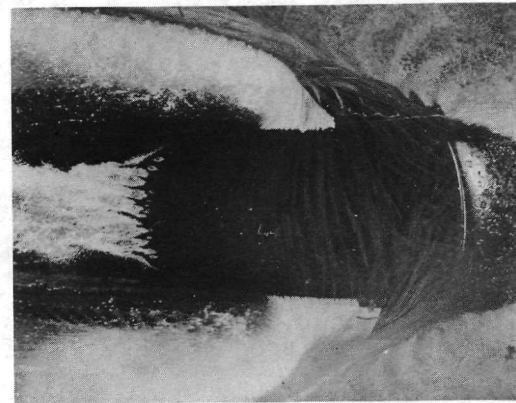
(d) $V = 45.7$ knots; $V/V_H = 0.98$; $\omega/\omega_O = 1$.
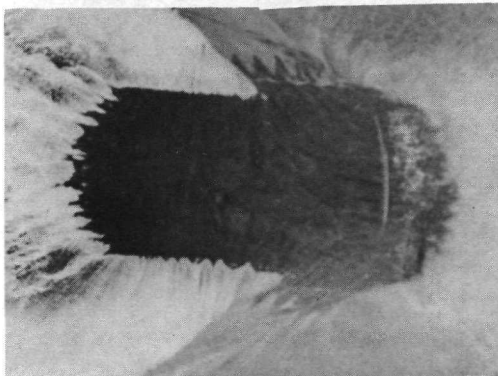
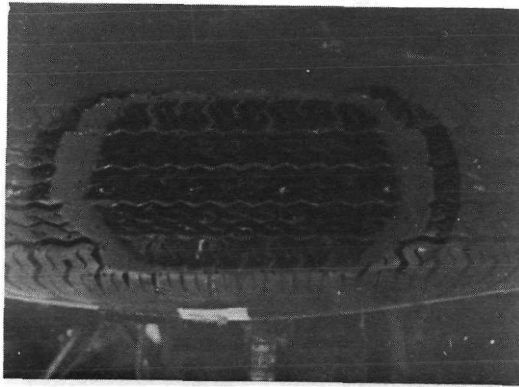(e) $V = 51.6$ knots; $V/V_H = 1.10$; $\omega/\omega_O < 1$.
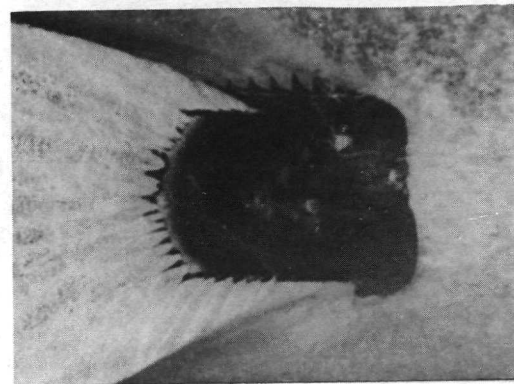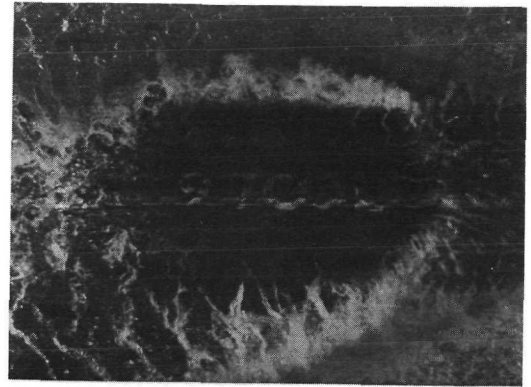
(f) $V = 70.0$ knots; $V/V_H = 1.50$; $\omega/\omega_O < 1$.
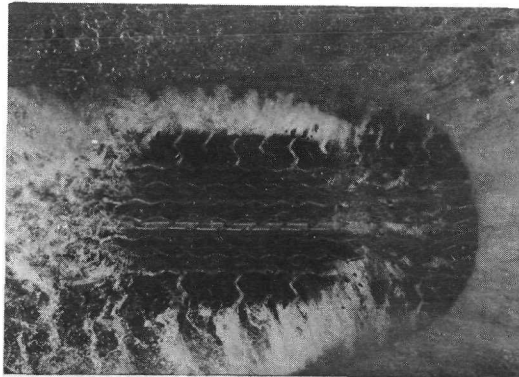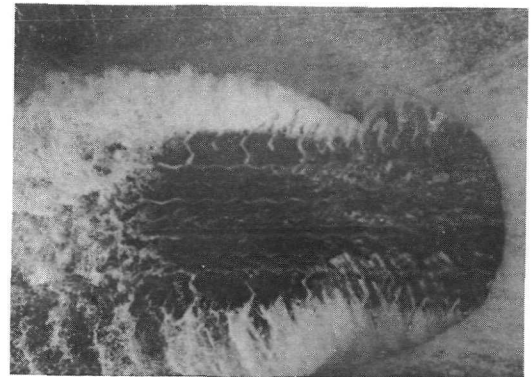
Direction of travel ⟶

L-72-6524

Figure 19.- Water action in footprint of smooth tire at $d = 10$ mm $(0.4$ in.$)$. $\psi = 4.5^O$; $p = 18.6$ N/cm^2 $(27$ lb/in$^2)$; $F_V = 3.71$ kN $(835$ lb$)$.

31
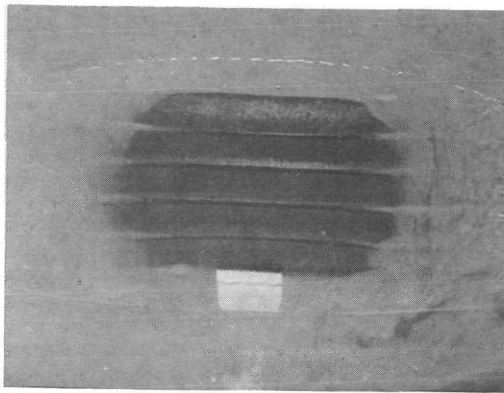
(a) Tire at rest.

(b) V = 19.8 knots; V/V_H = 0.42;
ω/ω_o = 1.

(c) V = 35.4 knots; V/V_H = 0.76;
ω/ω_o = 1.

(d) V = 36.0 knots; V/V_H = 0.77;
ω/ω_o = 1.

(e) V = 54.4 knots; V/V_H = 1.16;
ω/ω_o < 1.

(f) V = 76.3 knots; V/V_H = 1.63;
ω/ω_o < 1.

Direction of travel ⟶

Figure 20.- Water action in footprint of four-groove tire at   d = 10 mm (0.4 in.).
ψ = 4.5°;   p = 18.6 N/cm^2 (27 lb/in^2); F_V = 3.71 kN (835 lb).
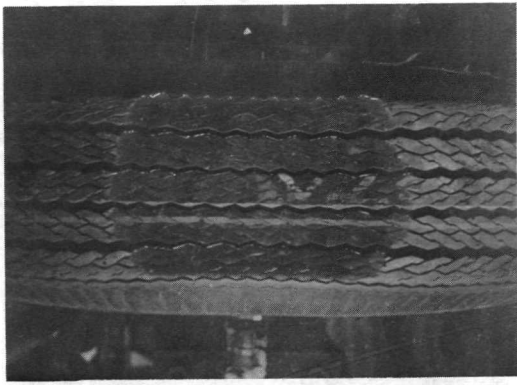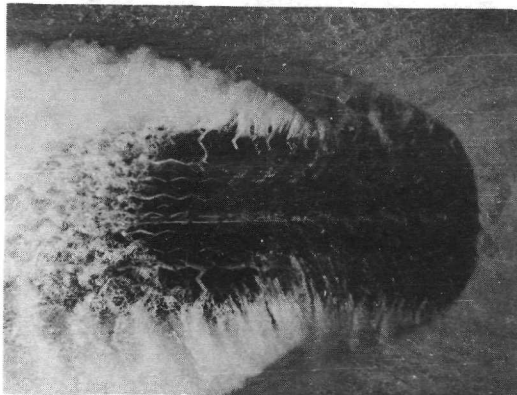
(a) Tire at rest.
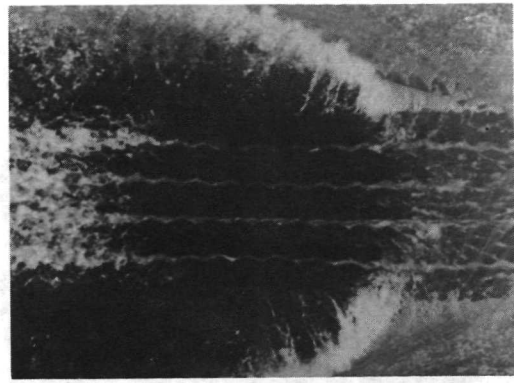
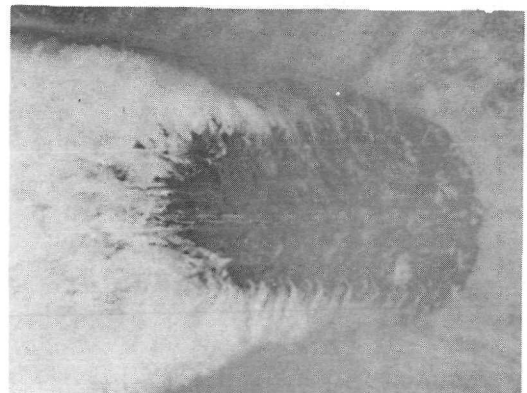(b) $V = 18.6$ knots; $V/V_H = 0.40$; $\omega/\omega_0 = 1$.

(c) $V = 32.8$ knots; $V/V_H = 0.70$; $\omega/\omega_0 = 1$.

(d) $V = 42.7$ knots; $V/V_H = 0.91$; $\omega/\omega_0 = 1$.
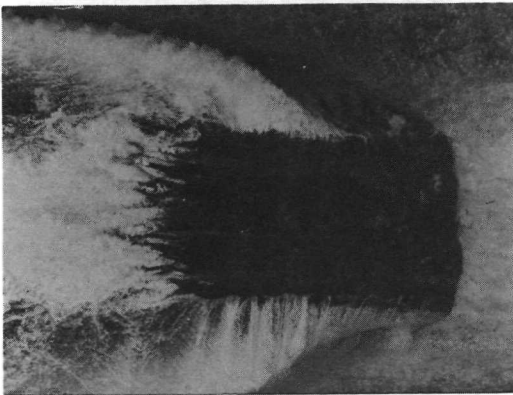
(e) $V = 51.4$ knots; $V/V_H = 1.10$; $\omega/\omega_0 < 1$.

(f) $V = 62.8$ knots; $V/V_H = 1.34$; $\omega/\omega_0 < 1$.
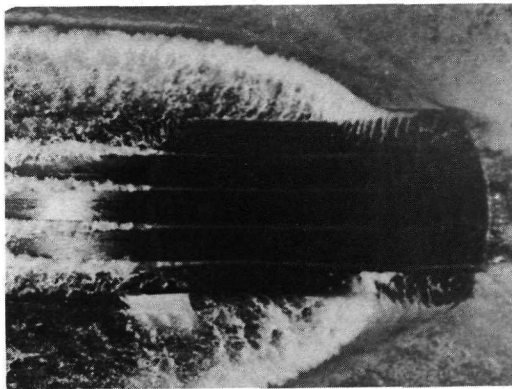
Direction of travel ⟶

L-72-6526

Figure 21.- Water action in footprint of production tire at $d = 10$ mm (0.4 in.) $\psi = 4.5^0$; $p = 18.6$ N/cm^2 (27 lb/in^2); $F_V = 3.71$ kN (835 lb).

(a) Tire at rest.

(b) $V = 17.0$ knots; $V/V_H = 0.36$; $\omega/\omega_o = 1$.

(c) $V = 36.9$ knots; $V/V_H = 0.79$; $\omega/\omega_o = 1$.

(d) $V = 43.0$ knots; $V/V_H = 0.92$; $\omega/\omega_o = 1$.

(e) $V = 51.3$ knots; $V/V_H = 1.10$; $\omega/\omega_o < 1$.

(f) $V = 64.8$ knots; $V/V_H = 1.38$; $\omega/\omega_o < 1$.

Direction of travel ⟶

L-72-6527

Figure 22.- Water action in footprint of experimental radial-ply tire at $d = 10$ mm
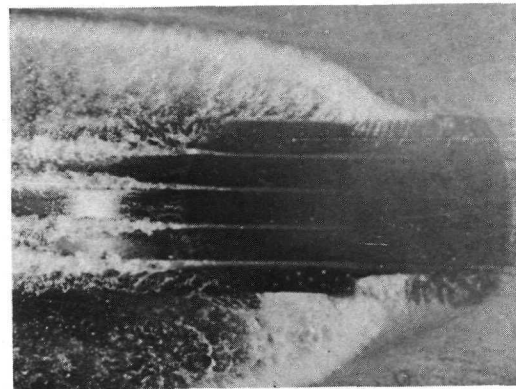(0.4 in.). $\psi = 4.5^o$; $p = 18.6$ N/cm^2 (27 lb/in^2); $F_V = 3.71$ kN (835 lb).
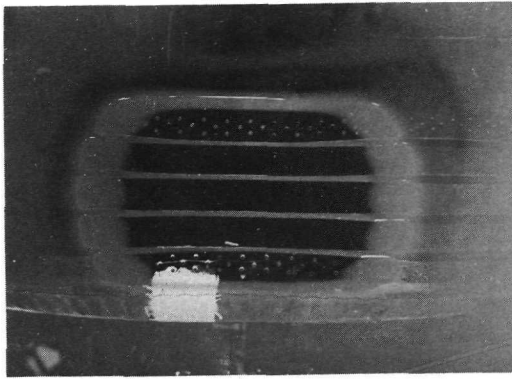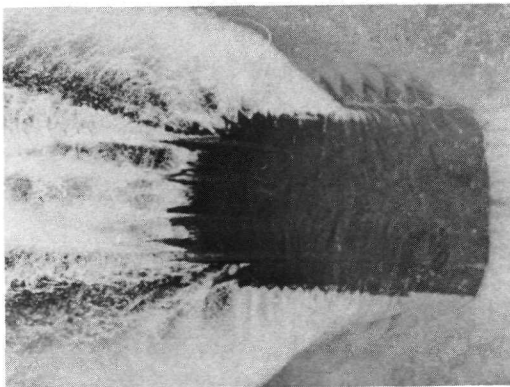
(a) Tire at rest.
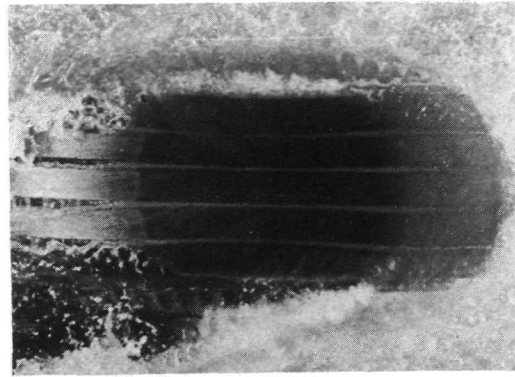
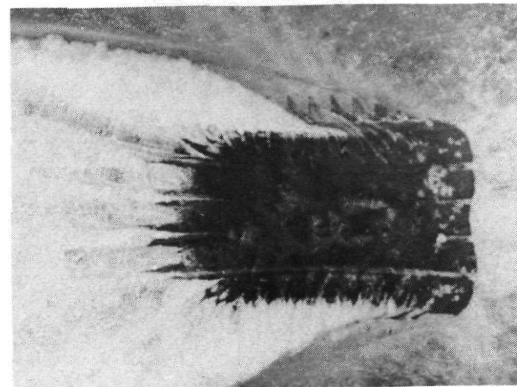(b) V = 11.7 knots; $V/V_H = 0.25$;
$\omega/\omega_O = 1.$

(c) V = 38.2 knots; $V/V_H = 0.82$;
$\omega/\omega_O = 1.$

(d) V = 42.6 knots; $V/V_H = 0.91$;
$\omega/\omega_O = 1.$

(e) V = 52.6 knots; $V/V_H = 1.12$;
$\omega/\omega_O < 1.$
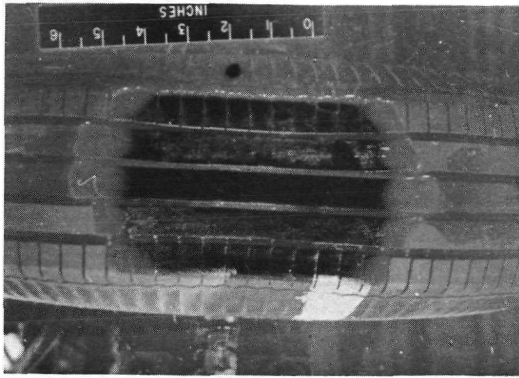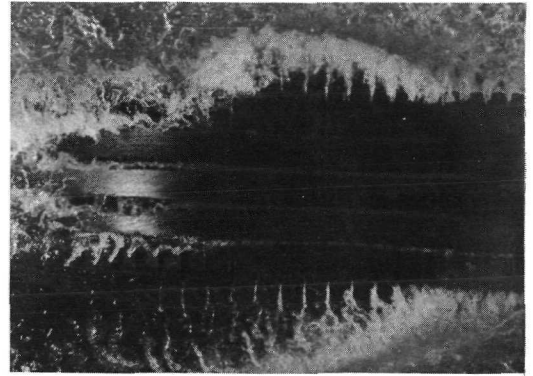
(f) V = 63.0 knots; $V/V_H = 1.35$;
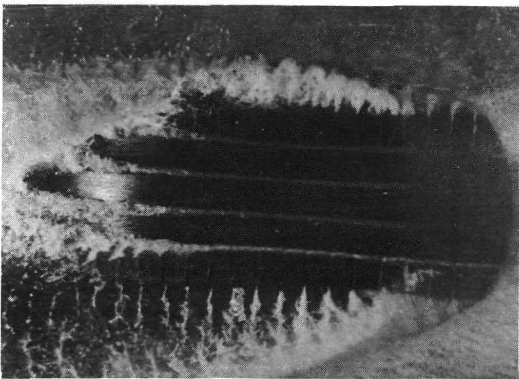$\omega/\omega_O < 1.$

Direction of travel ⟶

L-72-6528

Figure 23.- Water action in footprint of four-groove dimpled tire at   d = 10 mm (0.4 in.).
$\psi = 4.5^O$; p = 18.6 N/cm^2 (27 lb/in^2); F_V = 3.71 kN (835 lb).
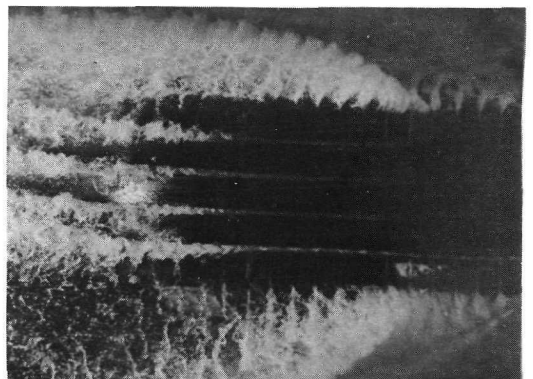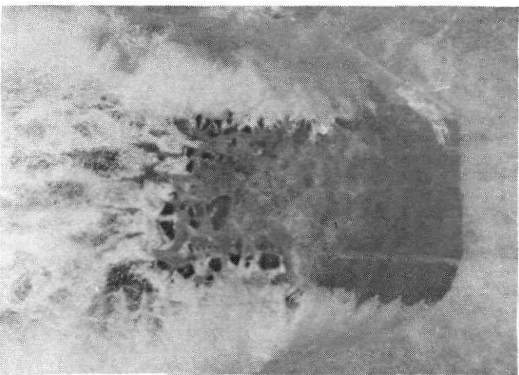
(a) Tire at rest.

(b) $V = 17.9$ knots; $V/V_H = 0.38$; $\omega/\omega_O = 1$.
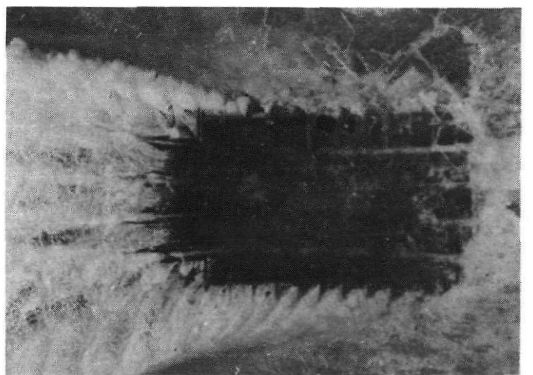
(c) $V = 36.8$ knots; $V/V_H = 0.79$; $\omega/\omega_O = 1$.

(d) $V = 42.8$ knots; $V/V_H = 0.91$; $\omega/\omega_O = 1$.

(e) $V = 52.7$ knots; $V/V_H = 1.13$; $\omega/\omega_O < 1$.

(f) $V = 72.6$ knots; $V/V_H = 1.55$; $\omega/\omega_O < 1$.

Direction of travel ⟶

L-72-6529

Figure 24.- Water action in footprint of four-groove slotted tire at $d = 10$ mm (0.4 in.).
$\psi = 4.5^O$; $p = 18.6$ N/cm^2 (27 lb/in^2); $F_V = 3.71$ kN (835 lb).

"The aeronautical and space activities of the United States shall be conducted so as to contribute . . . to the expansion of human knowledge of phenomena in the atmosphere and space. The Administration shall provide for the widest practicable and appropriate dissemination of information concerning its activities and the results thereof."
—NATIONAL AERONAUTICS AND SPACE ACT OF 1958

NASA SCIENTIFIC AND TECHNICAL PUBLICATIONS

TECHNICAL REPORTS: Scientific and technical information considered important, complete, and a lasting contribution to existing knowledge.

TECHNICAL NOTES: Information less broad in scope but nevertheless of importance as a contribution to existing knowledge.

TECHNICAL MEMORANDUMS: Information receiving limited distribution because of preliminary data, security classification, or other reasons. Also includes conference proceedings with either limited or unlimited distribution.

CONTRACTOR REPORTS: Scientific and technical information generated under a NASA contract or grant and considered an important contribution to existing knowledge.

TECHNICAL TRANSLATIONS: Information published in a foreign language considered to merit NASA distribution in English.

SPECIAL PUBLICATIONS: Information derived from or of value to NASA activities. Publications include final reports of major projects, monographs, data compilations, handbooks, sourcebooks, and special bibliographies.

TECHNOLOGY UTILIZATION PUBLICATIONS: Information on technology used by NASA that may be of particular interest in commercial and other non-aerospace applications. Publications include Tech Briefs, Technology Utilization Reports and Technology Surveys.

Details on the availability of these publications may be obtained from:

SCIENTIFIC AND TECHNICAL INFORMATION OFFICE

NATIONAL AERONAUTICS AND SPACE ADMINISTRATION
Washington, D.C. 20546